



ÉCOLE POLYTECHNIQUE  
FÉDÉRALE DE LAUSANNE

## Politecnico di Torino

Collegio di Ingegneria Elettronica, delle Telecomunicazioni e  
Fisica (ETF)

Master's degree program in:  
NANOTECHNOLOGIES FOR ICTs

*Master Thesis*

# A reconfigurable analog base-band amplifying filter for the Internet-of-Things based on Source Follower architectures

*Author*

Salvatore Collura

*Supervisors*

Luciano Scaltrito  
Fabrizio Bonani

*EPFL tutors*

Christian Enz  
Alessandro Pezzotta

September 2018



## Abstract

In the last 50 years, a lot of work has been made in order to develop what is now commonly known as Internet. The goal of internet has been to connect all the computing devices among each other, from desktop computer to smartphone. Now, more than half of the world population can connect to Internet and there are many efforts to increase this portion. Recently the challenge of “Internet-of-Things” (IoT) has been to connect not only computing devices but also all commonly used objects to each other. The current trend in technology shows that IoT has the potential to reshape how people interact with their daily environment.

To enable the spread of IoT devices one key challenge is the communication among the devices. Wireless communication is, by the user standpoint, far more convenient with respect to traditional wired connections. However, wireless devices suffer from higher power consumption and lower data transfer rate with respect to the wired counterpart. In addition, reliability issues can come up when multiple devices try to communicate to each other. The analog front-end dominates the power consumption in current Integrated Circuits (IC) for wireless IoT. Therefore, it is critical to optimize the power consumption of this part.

The next-generation WiFi standard (802.11ax) is one of the possible solution to these problems. It aims to increase the performance and the efficiency of data sharing among devices.

The goal of this work is to design a Low-Pass Filter (LPF) for an analog receiver compliant with the 802.11ax standard. The designed block is a sixth order Chebyshev Type I LPF composed of three different biquadratic cells, each one implementing a couple of complex-conjugate poles. The filter works in the high frequency range and it is capable to reconfigure its cut-off frequency between 10 MHz and 20 MHz. The Source follower (SF) architecture was used to implement the filter. The first cell is based on a new variant of the Flipped SF that is capable of amplification of the signal in the pass band. The second and third cells are both based on a new variant of the Super SF capable of obtaining very high quality factor. The filter was designed using the 28 nm technology provided by TSMC. The EKV model and Inversion-Coefficient-based (IC) design methodology was used in order to target low power application.

After post layout simulation, the filter is compliant with the 802.11ax standard. The power consumption of the system ranges between 50  $\mu$ W (for cut-off frequency of 10 MHz) and 120  $\mu$ W (for cut-off frequency of 20 MHz). The total area of the system is 0.015 mm<sup>2</sup>.



# Acknowledgements

I would like to thank professor Christian Enz for letting me joining the ICLAB group and for providing me with all the tools I needed to comfortably carry-out my project.

I would like to express my gratitude to Alessandro Pezzotta who guided me throughout this project and helped me numerous times with his experience.

I would like to thank Francesco Chicco and Raffaele Capoccia for their valuable suggestions for my work.

I would also like to thank all the people in ICLAB for the warm and calm environment I found in Microcity.

Special thanks also to Mattia, Vladimir and Sammy for their quick reflexes and characteristic skills.



# Contents

<b>1</b>	<b>Introduction</b>	<b>1</b>
<b>2</b>	<b>Wi-Fi standards - IEEE 802.11</b>	<b>4</b>
2.1	Introduction . . . . .	4
2.2	Standard Definitions . . . . .	4
2.3	PHY Standard introduction . . . . .	5
2.4	Receiver Specifications . . . . .	6
2.5	Transmitter specifications . . . . .	9
2.5.1	Towards 802.11ax . . . . .	9
<b>3</b>	<b>Transceiver architecture and filter requirements</b>	<b>12</b>
3.1	Introduction . . . . .	12
3.2	Transceiver architecture . . . . .	12
3.3	Filter requirements . . . . .	14
3.3.1	Towards 802.11ax . . . . .	17
3.4	Required Filter . . . . .	20
<b>4</b>	<b>Base-band filters and source follower state-of-the-art</b>	<b>22</b>
4.1	Introduction . . . . .	22
4.2	Filter topologies . . . . .	22
4.2.1	Continuous-time filters . . . . .	22
4.2.2	Discrete-time filters . . . . .	23
4.3	Source-Follower (SF) filters . . . . .	23
4.3.1	Super SF . . . . .	25
4.3.2	Flipped SF . . . . .	27
4.3.3	Cross-coupled SF . . . . .	28
<b>5</b>	<b>Proposed configuration</b>	<b>32</b>
5.1	Introduction . . . . .	32
5.2	Ideal filter parameters . . . . .	32
5.2.1	Parameters values . . . . .	33
5.3	Filter schematics and small signal models . . . . .	33
5.3.1	Small signal model . . . . .	36
5.3.2	Design challenges . . . . .	38
5.3.3	Quality factor . . . . .	39
5.4	Model and workflow . . . . .	39
5.4.1	Design methodology . . . . .	40
5.5	Filter sizing - 10 MHz . . . . .	41
5.5.1	From 10 to 20 MHz . . . . .	41

<b>6</b>	<b>Layout design</b>	<b>44</b>
6.1	Introduction . . . . .	44
6.2	Layout rules . . . . .	44
6.3	Layout implementation . . . . .	45
6.3.1	Cell 1 . . . . .	46
6.3.2	Cell 2 and 3 . . . . .	47
6.3.3	Complete layout . . . . .	48
<b>7</b>	<b>Results</b>	<b>51</b>
7.1	Introduction . . . . .	51
7.2	Post-layout results . . . . .	51
7.3	Comparison with Wi-Fi requirements . . . . .	52
7.4	Comparison with state-of-the-art . . . . .	60
<b>8</b>	<b>Conclusion</b>	<b>63</b>
8.1	Performance . . . . .	63
8.2	Future improvements . . . . .	64
8.3	Next steps . . . . .	64
<b>A</b>	<b>Matlab design and sizing</b>	<b>66</b>



# List of Figures

2.1	Sub-carriers diagram in a standard 20 MHz channel. There are displayed <b>data</b> sub-carriers and <b>pilot</b> sub-carriers. Null sub-carriers are also part of the channel. Figure taken from [3]. . . . .	6
2.2	BPSK and QPSK modulation . . . . .	7
2.3	Constellation in a 16-QAM modulation. . . . .	7
3.1	Basic Transceiver diagram with all its most relevant blocks. . . . .	13
3.2	Transmitter diagram with all its basic components [4]. . . . .	13
3.3	Receiver diagram with all its basic components [4]. . . . .	14
3.4	Low-Pass Prototype ( <b>LPP</b> ) plot, attenuation on the vertical axis and relative frequency on the horizontal one [5]. . . . .	15
4.1	First order Low-Pass Filter (LPF) based on source-follower [12] . . . . .	23
4.2	second order LPF based on the degenerate source-follower . . . . .	24
4.3	second order LPF based on the Super source-follower [13] . . . . .	25
4.4	small signal analysis for the circuit in Figure 4.3 . . . . .	26
4.5	second order LPF based on the Flipped source-follower [14] . . . . .	27
4.6	small signal analysis for the circuit in Figure 4.5 . . . . .	28
4.7	second order LPF based on the Flipped source-follower [12] . . . . .	29
4.8	differential small signal analysis for the circuit in Figure 4.7 . . . . .	29
5.1	The three second order transfer functions required by the sixth order Chebyshev LPF. . . . .	33
5.2	Sixth order Chebyshev LPF and Mask requirements. . . . .	34
5.3	General diagram of 6th order Chebyshev LPF. . . . .	34
5.4	Cell 1 - Amplifying fully-differential biquadratic cell based on Flipped SF. . . . .	35
5.5	Cell 2 - Fully-differential biquadratic cell based on Super SF. . . . .	35
5.6	Cell 3 - Fully-differential biquadratic cell based on Super SF. . . . .	36
5.7	Small signal model for Cell 1. . . . .	36
5.8	Small signal model for Cell 2 and 3. . . . .	37
5.9	Workflow used to size the first cell. . . . .	41
5.10	Implementation of resistor $R_1$ , where $R = 825 \Omega$ . . . . .	42
5.11	Implementation of resistor $R_2$ , where $R = 825 \Omega$ . . . . .	42
6.1	Layout of the first cell without capacitors, transistors at the bottom part of the centre, system of resistances at the sides and at top part of the centre. . . . .	46
6.2	Layout of the second cell without capacitors. . . . .	47
6.3	Layout of the third cell without capacitors. . . . .	48

6.4	Complete layout of the sixth order LPF . . . . .	49
7.1	<b>Ideal</b> vs <b>post layout</b> amplitude transfer function of the first biquadratic cell, when cut-off frequency of the filter is set to 10 MHz. . . . .	53
7.2	<b>Ideal</b> vs <b>post layout</b> amplitude transfer function of the first biquadratic cell, when cut-off frequency of the filter is set to 20 MHz. . . . .	53
7.3	<b>Ideal</b> vs <b>post layout</b> amplitude transfer function of the second biquadratic cell, when cut-off frequency of the filter is set to 10 MHz. . . . .	54
7.4	<b>Ideal</b> vs <b>post layout</b> amplitude transfer function of the second biquadratic cell, when cut-off frequency of the filter is set to 20 MHz. . . . .	54
7.5	<b>Ideal</b> vs <b>post layout</b> amplitude transfer function of the third biquadratic cell, when cut-off frequency of the filter is set to 10 MHz. . . . .	55
7.6	<b>Ideal</b> vs <b>post layout</b> amplitude transfer function of the third biquadratic cell, when cut-off frequency of the filter is set to 20 MHz. . . . .	55
7.7	<b>Ideal</b> vs <b>post layout</b> amplitude transfer function of the entire system, when cut-off frequency of the filter is set to 10 MHz. . . . .	56
7.8	<b>Ideal</b> vs <b>post layout</b> amplitude transfer function of the the entire system, when cut-off frequency of the filter is set to 20 MHz. . . . .	56
7.9	Detail of the pass band ripple of Figure 7.7. . . . .	57
7.10	Detail of the pass band ripple of Figure 7.8. . . . .	57
7.11	<b>Ideal</b> vs <b>post layout</b> phase transfer function of the entire system in linear scale, when cut-off frequency of the filter is set to 10 MHz. . . . .	58
7.12	<b>Ideal</b> vs <b>post layout</b> amplitude transfer function of the the entire system in linear scale, when cut-off frequency of the filter is set to 20 MHz. . . . .	58
7.13	Input referred noise ( $\mu\text{V}/\sqrt{\text{Hz}}$ ) of the system for <b>10 MHz</b> and <b>20 MHz</b> . . . . .	59
7.14	Detail of the input referred noise shown in Figure 7.13. . . . .	59



# List of Tables

2.1	Minimum input level Sensitivity ( <b>MS</b> ) in dBm. . . . .	8
2.2	Adjacent Channel Rejection ( <b>ACR</b> ) and Non-adjacent Channel Rejection ( <b>NCR</b> ) in dB. . . . .	8
2.3	Maximum input level in dBm. . . . .	9
2.4	Maximum allowed relative constellation error in dB. . . . .	9
3.1	802.11ax standard Required Filter Order (RFO) for a given Band-Width (BW), pass band attenuation ( $A_P$ ) and Transition Band-Width (TBW). . . . .	19
4.1	Summary of Super SF filter characteristics . . . . .	26
4.2	Summary of Cross-coupled SF filter characteristics . . . . .	30
5.1	Values of the quality factor $Q$ and the cut-off frequency multiplier $F_r$ for each cell of the final sixth order Chebyshev LPF. They are valid for both 10 MHz and 20 MHz. . . . .	33
5.2	Values of all the components in Cell 1, 2 and 3 for a cut-off frequency of 10 MHz. . . . .	41
5.3	Required variation in parameters for cut-off frequency of 10 MHz and 20 MHz. . . . .	42
7.1	Comparison of the characteristics of the simulated filter with respect to the measurements from the state-of-the-art . . . . .	61



# Chapter 1

## Introduction

This chapter presents a summary of all the content in this report.

Chapter 2 presents an overview of the IEEE 802.11 (Wi-Fi) standard focused on the Physical Layer (PHY). A basic introduction of the Wi-Fi standard is necessary in order to get familiarity with its background and definitions. First, the chapter focuses on the current standards (802.11 $n,ac$ ) and it presents the receiver and transmitter specifications that are relevant for this project. The most important ones are: maximum and minimum input level sensitivity, adjacent and non-adjacent channel rejection and relative constellation RMS error. The second part expands the specifications retrieved previously in order to include the next-generation standard (802.11 $ax$ ).

Chapter 3 presents the electronic background in order to understand the environment in which the LPF is used. First, basic schematics of a transceiver, receiver and transmitter are provided. Relying on the information in Chapter 2, the central part analyses the characteristics of a LPF in a general receiver such as: bandwidth, type, order, dynamic range, linearity and noise. In addition, it retrieves also the requirements for current standards (802.11 $n,ac$ ). As already done in Chapter 2, the analysis is expanded also for the 802.11 $ax$  standard. The last part summarises the feature required in a LPF targeting 802.11 $ax$  standard.

Chapter 4 presents an overview of the filter categories and topologies for Wi-Fi applications. The most relevant categories are  $G_m$ - $C$ , active-RC, Switched-Capacitor and Source Follower (SF) filters. SF filters are a new and promising topology for HF/VHF circuits. Then, the second part of this chapter provides an analysis of the current state-of-the-art of SF filters and of their major characteristics.

Chapter 5 proposes a configuration for the LPF required at the end of Chapter 3. In the first part, the parameters of an ideal filter are computed from the specifications in Chapter 3. The second part presents the schematic of a sixth order Chebyshev Type I filter based on SF. First a general diagram shows the three biquadratic cells that constitute the filter. Then, each of the three cells is presented at the circuit level. Cell 1 is a new implementation of an amplifying circuit based on the Flipped SF. Cell 2 and 3 are a new implementation of Super SF capable to achieve high quality factors. Another relevant feature of this filter is the capability of changing the bandwidth from 10 to 20 MHz. The small signal model is analysed and an overview of the design trade-off is presented. The third part provides an explanation of the design methodology and a quick overview of the EKV model used in the design stage. The last part presents the final sizing of the components for both bandwidths

designed in this work.

Chapter 6 completes the schematics presented in Chapter 5 implementing their layouts. A series of good layout rules are provided in order to reduce mismatch among transistors and to rout efficiently different components. A layout for each biquadratic cell is presented and analysed as well as the complete filter layout at the end of the chapter.

Chapter 7 presents the results retrieved from the post-layout simulations. In addition, it compares them with the 802.11ax requirements presented in Chapter 3. The last part compares the simulated results with the state-of-the-art of Source Follower,  $G_m$ - $C$  and active-RC filters.

Chapter 8 concludes this work by summarising the performance of the filter and by highlighting the possible improvements in the future as well as the next steps of this project.



# Chapter 2

## Wi-Fi standards - IEEE 802.11

### 2.1 Introduction

This chapter presents an overview of the Physical layer (*PHY*) in Wi-Fi standards (*a, b, g, n, ac*) [1] and drafts (*ax*) [2]. In addition it analyses also the receiver and transmitter specifications.

The first part presents an introduction of the Wi-Fi standard as well as some basic definitions. The second part explains all the specifications of a receiver and a transmitter that are relevant for the design of a low-pass filter compliant with 802.11*n* and 802.11*ac* standards. The third part will extend the analysis also for the 802.11*ax* (Draft 2.1) which is not completely standardised yet.

802.11*n/ac* provide the highest performance and, consequently, they have more stringent requirements during the design phase. Furthermore, the 802.11*ax* standard will explicitly require backward compatibility with 802.11*n/ac*.

In addition, the two standards are backward compatible with the previous ones: 802.11*a*, 802.11*b* and 802.11*g*. Then, all the standards currently used on the market are respected if the device is compliant with both 802.11*n* and 802.11*ac*. The 802.11*n* provides backward compatibility with 802.11*a/b/g* since it works in two frequency ranges, 2.4 GHz and 5 GHz. The 802.11*ac* is the newest and most efficient standard, it provides backward compatibility with the 802.11*a* standard because it works only in the 5 GHz frequency range.

### 2.2 Standard Definitions

Some definitions must be given before diving deeper in the specification.

- The Physical Layer (*PHY*) Defines all the physical and electrical requirements for a device in order to correctly transmit data over a medium. It establishes and terminates the connection, it manages the sharing of the resources over multiple users and it treats (modulates) the signal so to make it compliant with the transmission medium.
- The PHY Layer Convergence Procedure (*PLCP*) is one of the sub-layer of the *PHY* and it adapts the packets depending on the used physical layer. It is also responsible for the *CCA* mode.

- The PLCP protocol data unit (*PPDU*) is the product of the *PLCP*. It contains all the information that must be transmitted in a form compatible with the *PHY*. It contains three sections: preamble, header and data.
- The Physical Layer Service Data Unit (*PSDU*) is the content (data) of the *PPDU*.
- The Packet Error Ratio (*PER*) is the ratio of erroneous packet over the total number of packet received.
- The Clear Channel Assessment (*CCA*) is the system that allows to establish if a carrier is free or occupied. It is subdivided in *CCA-CS* and *CCA-ED*.
- The Clear Channel Assessment - Carrier Sense (*CCA-CS*) is used to sense the power transmitted in a carrier. This mechanism activates once the received power is above a specified threshold, meaning that the carrier is being used.
- Clear Channel Assessment - Energy Detect (*CCA-ED*) is used to sense the power in a carrier coming from all the non-WiFi sources. The transmission is paused when the power is above a specified threshold.
- Orthogonal Frequency Division Multiplexing (*OFDM*) is a type of digital modulation that targets high data rates by means of spreading the information over multiple sub-carriers.
- Direct Sequence Spread Spectrum (*DSSS*) is a type of digital modulation used in the first implementations of the Wi-Fi protocol. The information is transported by only one carrier which takes the whole available channel.

## 2.3 PHY Standard introduction

The *IEEE 802.11* is the standard which stands as the foundation of the well known Wi-Fi. The first version of the Wi-Fi, the 802.11, was announced in 1997 and in a bit more of 20 years it has become ubiquitous. Successive standards aimed to increase the performance and the efficiency of this wireless communication. Following the release order, the main updates are: 802.11b in 1999, 802.11a in 1999, 802.11g in 2003, 802.11n in 2009, 802.11ac in 2013. The preferred Radio Frequency (RF) used by these standards is either 2.4 GHz or 5 GHz. Depending on the country, the maximum allotted bandwidth is usually smaller than 100 MHz in the case of 2.4 GHz. 5 GHz frequencies allows to increase the bandwidth to no more than 200 MHz. The allotted bandwidth is divided in multiple sub-bands or channels. Channels have a minimum width of 20 MHz, this width varies depending on the standard used. For example, 40 MHz channels are supported by 802.11n while 802.11ac supports also channels of 80 MHz and 160 MHz

802.11 and 802.11b use *DSSS* to transfer information from a transmitter to a receiver. 802.11a,g,n,ac replace *DSSS* with the more efficient *OFDM*. In *OFDM* the high data rate of digital stream is divided in  $N$  number of sub-streams that have an equivalent data rates divided by  $N$ . Since the each sub-stream have a lower data rate it implies that also its spectrum will be thinner. It is then possible to place multiple sub-stream close to each other in the same allotted channel as it is

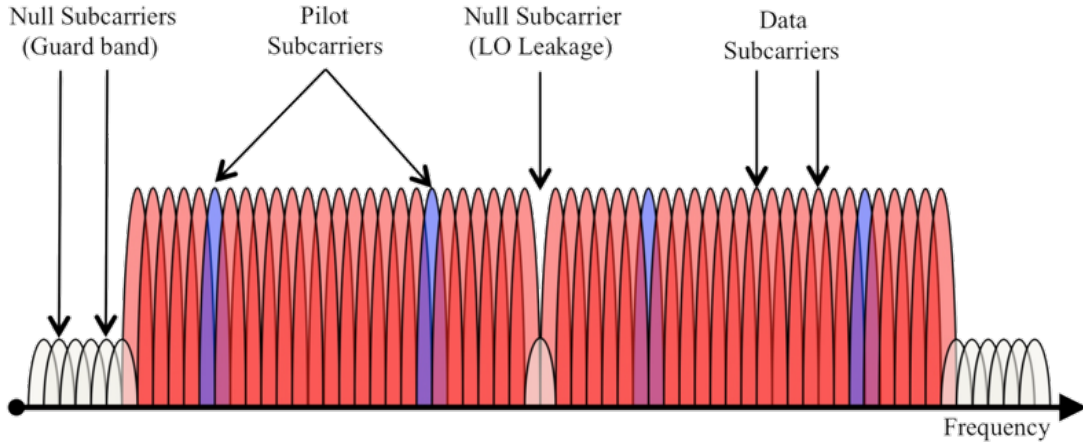


Figure 2.1: Sub-carriers diagram in a standard 20 MHz channel. There are displayed **data** sub-carriers and **pilot** sub-carriers. Null sub-carriers are also part of the channel. Figure taken from [3].

displayed in Figure 2.1. In Figure 2.1 data sub-carriers are coloured in red. The standard requires some pilot sub-carriers (in blue) that are used to better handle the channel during the digital data processing. In the channel there are also sub-carriers that are not used because it is required to make some distance between two adjacent channels in order to reduce noise coming from other channels.

The efficiency of the communication is almost always related by the amount of data that can be transferred by each sub-carrier. For this reason, many different types of modulations have been standardized. The main reason for the different types of modulations is the trade-off between reliability and throughput. In fact, the more data are packed in a sub-carrier the more they can be degraded by noise. In order of reliability, the main types of modulations are: Binary Phase Shift Keying (BPSK), Quadrature Phase Shift Keying (QPSK), Quadrature and Amplitude Modulation (QAM). The most performing is the QAM which is further divided in 16-64-256-QAM depending on the number of points, called constellation, that the modulation can consider. Each point on the constellation is an unique combination of a signal amplitude (I) and phase (Q). The difference among BPSK, QPSK and 16-QAM is shown in Figure 2.2 and Figure 2.3.

## 2.4 Receiver Specifications

All the required signal specifications for a receiver (802.11n,ac) are listed below:

1. **Minimum input level sensitivity:** The minimum input level at the receiving antenna that provides a *PER* smaller than 10% for a *PSDU* of 4096 bytes.
2. **Maximum input level:** The allowed maximum input level at the receiver antenna that provides a *PER* smaller than 10% for a *PSDU* of 4096 bytes.
3. **Adjacent channel rejection:** It is the minimum ratio between the power of an adjacent channel over the power of the carrier channel which provides a

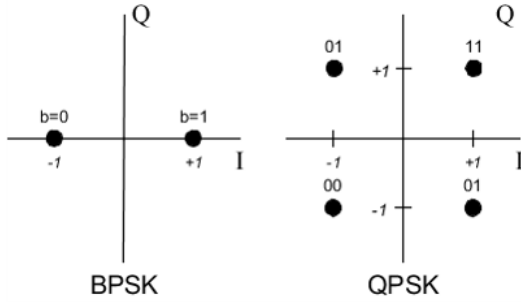


Figure 2.2: BPSK and QPSK modulation

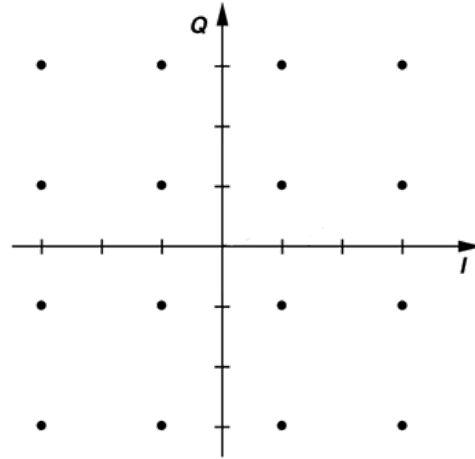


Figure 2.3: Constellation in a 16-QAM modulation.

$PER$  smaller than 10% for a  $PSDU$  of 4096 bytes. In order to compute this parameter the two channels must have the same bandwidth and the centre frequencies of the two channels must be separated by the bandwidth of the channels. The signal must be fixed to a constant power, 3 dB higher than its equivalent minimum input level sensitivity.

4. **Non-adjacent channel rejection:** Same definition as the “Adjacent channel rejection” but in this parameter the two channel centre frequencies must be separated by twice the bandwidth of the channels at least.
5. **CCA sensitivity:** Bandwidth-referred thresholds indicating the maximum power that must be present in a carrier to guarantee the correct transmission of a packet ( $PER$  smaller than 10% for a  $PSDU$  of 4096 bytes).
6. **Received Channel Power Indicator ( $RCPI$ ):** It is the measurement of the received power in the channel which carries the signal. The power is measured only over the  $PSDU$  and it is averaged over all the receiving chains. Parameter used in 802.11n standard.
7. **Reduced Interframe Space ( $RIFS$ ):** Time interval that separate two different packet transmissions. Parameter used in 802.11n standard.
8. **Received Signal Strength Indicator ( $RSSI$ ):** Similarly to  $RCPI$ , it is a measurement of the power of the signal taken in account. Parameter used in 802.11ac standard.

All these parameters are important for the correct implementation of the 802.11 standards. However, on the context of filters design only some of them are relevant. The focus of this report will be centred toward the first four parameters.

Table 2.1 and Table 2.2 summarise respectively the minimum input level sensitivity ( $MS$ ) and the adjacent/non-adjacent channel rejection ( $ACR$ ,  $NCR$ ) for both 802.11n and 802.11ac standards. The “Rate” in both tables represents the coding rate for which the data are encoded, it trades the throughput in favour of an

		802.11 $n,ac$		802.11 $ac$			
		Modulation	Rate	MS for 20 MHz channel	MS for 40 MHz channel	MS for 80 MHz channel	MS for 160, 80 + 80 MHz channel
802.11 $n,ac$		BPSK	1/2	-82	-79	-76	-73
		QPSK	1/2	-79	-76	-73	-70
		QPSK	3/4	-77	-74	-71	-68
		16-QAM	1/2	-74	-71	-68	-65
		16-QAM	3/4	-70	-67	-64	-61
		64-QAM	2/3	-66	-63	-60	-57
		64-QAM	3/4	-65	-62	-59	-56
802.11 $ac$		64-QAM	5/6	-64	-61	-58	-55
		256-QAM	3/4	-59	-56	-53	-50
		256-QAM	5/6	-57	-54	-51	-48

Table 2.1: Minimum input level Sensitivity (**MS**) in dBm.

		$n, ac$		$ac$			
		Modulation	Rate	ACR for 20,40,80,160 MHz channel	NCR for 20,40,80,160 MHz channel	ACR for 80+80 MHz channel	NCR for 80+80 MHz channel
$n$	$ac$	BPSK	1/2	16	32	13	29
		QPSK	1/2	13	29	10	26
		QPSK	3/4	11	27	8	24
		16-QAM	1/2	8	24	5	21
		16-QAM	3/4	4	20	1	17
		64-QAM	2/3	0	16	-3	13
		64-QAM	3/4	-1	15	-4	12
$ac$	$ac$	64-QAM	5/6	-2	14	-5	11
		256-QAM	3/4	-7	9	-10	6
		256-QAM	5/6	-9	7	-12	4

Table 2.2: Adjacent Channel Rejection (**ACR**) and Non-adjacent Channel Rejection (**NCR**) in dB.

increase in redundancy. Note that the MS in Table 2.1 is an absolute value (dBm), while the ACR/NCR in Table 2.2 are relative values (dB).

Table 2.1 reminds that 802.11 $n$  standard supports channel bandwidths of 20 and 40 MHz. 802.11 $ac$  increases the allowed bandwidths to 80 and 160 MHz.

802.11 $ac$  supports also the 256-QAM modulation. This increases the performance of the standard at the cost of a reduction of the channel tolerance on the interference from other channels (Table 2.2) and an increase of the minimum input level sensitivity (Table 2.1).

Table 2.3 presents the maximum input level allowed in a channel. This level is independent from the channel bandwidth and from the standard used.

	Band	Maximum input level
802.11n	2.4 GHz	-20
802.11n,ac	5 GHz	-30

Table 2.3: Maximum input level in dBm.

	Modulation	Rate	Relative constellation error
802.11n,ac	BPSK	1/2	-5
	QPSK	1/2	-10
	QPSK	3/4	-13
	16-QAM	1/2	-16
	16-QAM	3/4	-19
	64-QAM	2/3	-22
	64-QAM	3/4	-25
	64-QAM	5/6	-27
802.11ac	256-QAM	3/4	-30
	256-QAM	5/6	-32

Table 2.4: Maximum allowed relative constellation error in dB.

## 2.5 Transmitter specifications

It is important to understand some specifications of the transmitter so to better estimate the parameters used in the design of the filter in the receiver. This section will cover the following parameters:

- **Relative constellation RMS error:** It is the maximum error allowed in the modulated signal allowed from the standards. It is computed averaging the errors present in all the sub-carriers of all the channels in the allotted frequency bands. Section 5.3 will consider this parameter as the reciprocal of the minimum Signal-to-Noise Ratio (**SNR**) required at the input of the receiver.
- **Maximum transmit spectral flatness deviations:** It is the allowed variation in power of the sub-carriers with respect to the transmitted power. The tolerance varies depending on the position of the sub-carriers in the channel. In general, the sub-carriers near the central channel frequency can have  $\pm 4$  dB of variation. This range increases to  $[-6,+4]$  dB for the sub-carriers near the edges of channel.

Table 2.4 shows the maximum constellation error which the transmitter is allowed to produce over a channel. The number increase with the complexity of the modulation. This trend is reasonable since a larger set of constellation points means a smaller spacing among them, hence a smaller tolerance towards noise.

### 2.5.1 Towards 802.11ax

This section will briefly explain the differences and similarities between 802.11ax and 802.11n/ac standards. 802.11ax will be used in the frequencies of 2.4 GHz and 5 GHz. Hence, it will be compatible with both 802.11n/ac and the specifications of

the filter/receiver will follow the ones mentioned previously. *OFDM* and 1024-QAM will be used to transmit information over the carriers.

- **Minimum input level sensitivity:** For the same Rate, 1024-QAM will further increase the 256-QAM level of 6 dB for all the available bandwidths.
- **Maximum input level sensitivity:** This level remains equal to -30 dBm since 802.11ax will support both 802.11ac and 802.11n.
- **ACR and NCR:** For the same Rate, 1024-QAM will further reduce the 256-QAM level of 6 dB for all the available bandwidths.
- **Relative constellation RMS error:** For the same Rate, 1024-QAM will further reduce the 256-QAM level of 6 dB for all the available bandwidths.
- **Maximum transmit spectral flatness deviations:** 802.11ax is not going to change the values already available for 802.11ac and 802.11n.



# Chapter 3

## Transceiver architecture and filter requirements

### 3.1 Introduction

The first part of this chapter introduces basic notions about the structure of a transceiver. Once the transceiver structure is analysed, the chapter focuses on the Low-pass Filter (LPF) component of the receiver. The second part of the chapter presents the general parameters and specifications that an analog filter must satisfy in order to be compliant with the different 802.11 standards ( $a$ ,  $b$ ,  $g$ ,  $n$ ,  $ac$ ) and drafts ( $ax$ ). As a conclusion, the chapter presents the general characteristics that a LPF must have in order to be used in this topic.

### 3.2 Transceiver architecture

The transceiver is a system that allows the wireless communication between two Integrated Circuits (IC). The transceiver integrates the capabilities of wireless receivers and transmitters in a single component. A simplified version of a transceiver is presented in Figure 3.1 At the left of Figure 3.1 it is placed an antenna. In general, the transceiver is composed by one or multiple antennas which transform the Radio Frequency (RF) signal into an electric signal or vice versa. In this simplified model, the transceiver cannot receive and transmit information at the the same time. In fact, there is a Duplexer connected to the antenna which allows the use of the antenna to both the receiver part and the transmitter one, but not simultaneously. At the right of Figure 3.1 there is an Analog-to-Digital Converter (ADC) and a Digital-to-Analog Converter (DAC), components that allows to transfer data to/from the digital part of the receiver/transmitter.

Figure 3.2 shows the basic structure of a transmitter [4].

The goal of the circuit shown in Figure 3.2 is to encode the information contained in the  $I$  and  $Q$  signals into a RF signal. In order to accomplish this,  $I$  and  $Q$  must be summed together without any loss of information. This is done by shifting the phase of one of the signals ( $Q$ ) so that the two signals can be in phase quadrature. After the  $I$  and  $Q$  signals are summed, the signal is up-converted to the used RF by a mixer. A Band-Pass Filter (BPF) is used to filter out unwanted interferers. Before arriving to the antenna, the power of the signal is increased by a Power Amplifier

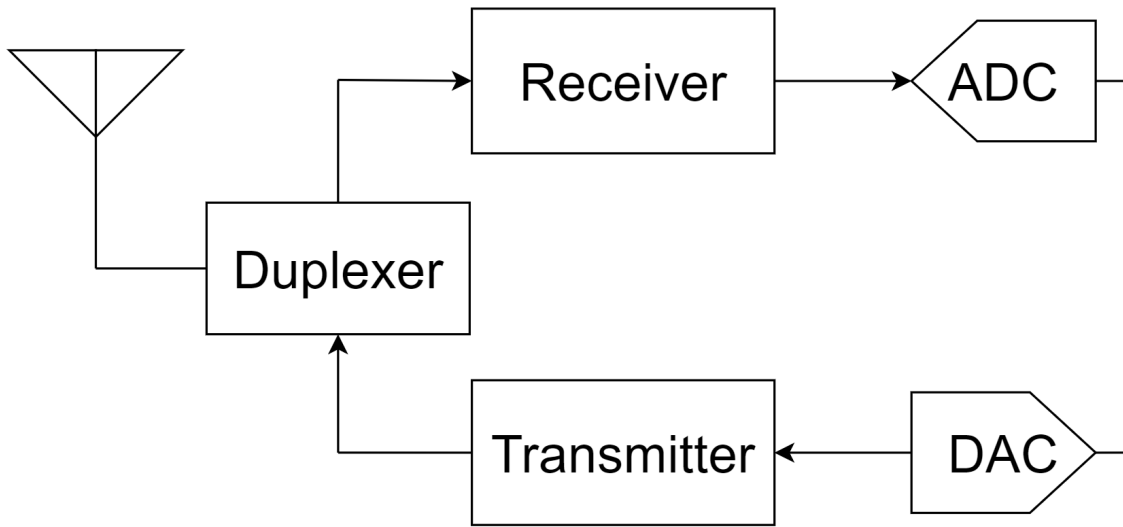


Figure 3.1: Basic Transceiver diagram with all its most relevant blocks.

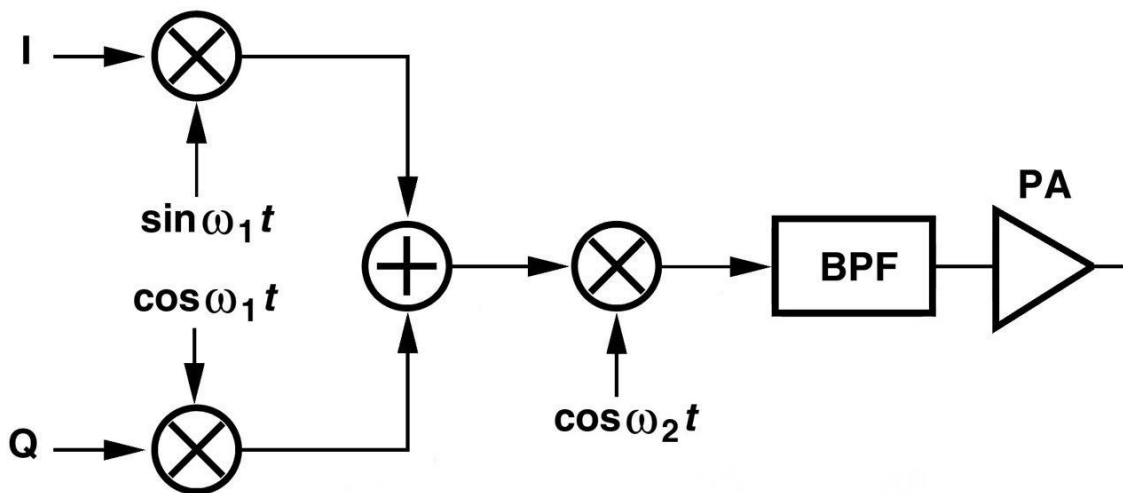


Figure 3.2: Transmitter diagram with all its basic components [4].

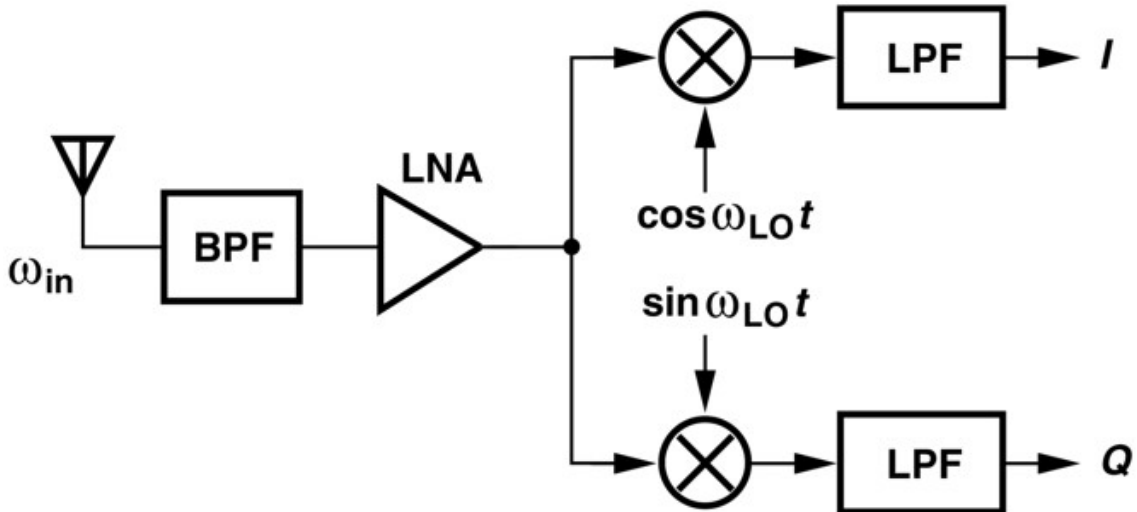


Figure 3.3: Receiver diagram with all its basic components [4].

(PA) so that data have enough strength to reach the receiver.

Figure 3.3 shows the basic structure of a receiver [4].

In Figure 3.3 the information coming from the antenna is first filtered by a BPF and then it is also amplified by a Low-Noise Amplifier (LNA). The signal is then split in two branches. For each branch there is a mixer used to down-convert either the amplitude ( $I$ ) or the phase ( $Q$ ) of the signal to a Low-Frequency (LF) or base-band. A Low-Pass Filter (LPF) selects only the frequencies carrying relevant information. After the LPF the signal can be converted in digital information through an ADC.

### 3.3 Filter requirements

From the previous section and taking in account the parameters listed in Chapter 2 it is possible to retrieve the requirements for a Low-Pass filter (LPF) compliant with the 802.11n,ac standard.

- **Bandwidth:** The analysed standards support bandwidths from 20 MHz to 160 MHz. These values refer to band-pass filters. It is possible to take advantage of the demodulator (e.g. using heterodyne techniques) to dynamically shift the frequencies of the channel near the zero frequency, so that it is possible to use a simpler LPF. In this case, the required bandwidths are divided by two and they range from 10 to 80 MHz.
- **Type and order:** 802.11n standard considers the minimum distance between the edges of two adjacent channels to be 5 MHz. 802.11ac standard, instead does not leave any space between the channels. However, in the latter case, not all the bandwidth of the channel is actively used. In fact, in a 20 MHz channel, only 16.6 MHz or 17.8 MHz are occupied by active *OFDM* sub-carriers.

This difference comes from the number of used sub-carriers inside one channel. 802.11a standard uses 52 sub-carriers out of the 64 available. 802.11ac enlarge this number to 56. Each sub-carrier has a bandwidth of 312.5 kHz.

Considering a symmetric distribution of the sub-carriers with respect to the centre frequency, it means that the space between two adjacent channels is

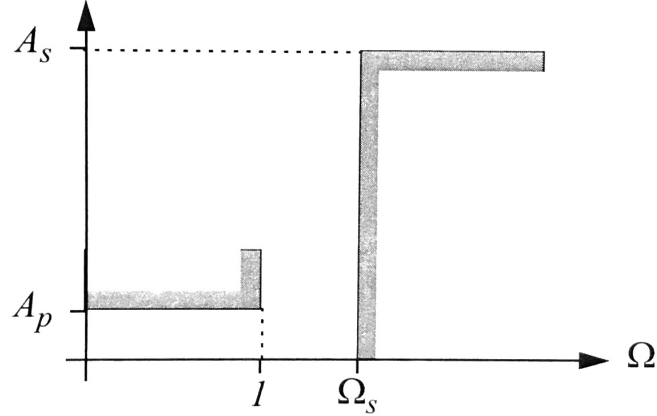


Figure 3.4: Low-Pass Prototype (**LPP**) plot, attenuation on the vertical axis and relative frequency on the horizontal one [5].

2.2 MHz in the worst case. This is obviously a tighter constraint than the one from 802.11n standard.

With the previous data it is now possible to retrieve the filter specifications. The worst case is found for BPSK modulation and 802.11ac standard, which require a stop-band attenuation  $A_S = 16$  dB. The stop-band relative frequency  $\Omega_S$  depends on the bandwidth of the channel. Referring to the null sub-carriers in Figure 2.1,  $\Omega_S$  depends on the frequencies at the edges of two neighbouring channels,  $\omega_{carrier,end}$  and  $\omega_{interferer,start}$ . As an example, it is presented the computation in the case of a 40 MHz channel.

$$\Omega_S = \frac{\omega_{interferer,start}}{\omega_{carrier,end}} = \frac{2\pi \cdot 21.7 \text{ MHz}}{2\pi \cdot 18.3 \text{ MHz}} = 1.18 \text{ rad/s}$$

Figure 3.4 shows the Low-Pass Prototype (LPP) for filter design. The vertical axis represent the attenuation, while the horizontal one represent the frequency in rad/s. To complete the requirements for the analysis of the filter it will be considered a maximum pass-band attenuation of  $A_P = 1$  dB.

The order of the filter is thus simply computed using the following formulas:

$$N = \frac{\log\left(\frac{10^{\frac{A_S}{10}} - 1}{10^{\frac{A_P}{10}} - 1}\right)}{2 \cdot \log(\Omega_S)} \quad (3.1)$$

$$N = \frac{\text{arcCosh}\left(\frac{\sqrt{10^{\frac{A_S}{10}} - 1}}{\sqrt{10^{\frac{A_P}{10}} - 1}}\right)}{\text{arcCosh}(\Omega_S)} \quad (3.2)$$

Equation 3.1 and Equation 3.2 give the minimum filter order required to respect the specifications. Equation 3.1 corresponds to a Butterworth filter, while Equation 3.2 corresponds to a Chebyshev one.

In general, the filter order depend on the value of  $A_P$ ,  $A_S$ , the maximum pass-band frequency and the minimum stop band frequency.

The **ACR** and **NCR** values in Table 2.2 impose that the larger is the out-of-band frequency filter the higher must be the attenuation. The worst case is for BPSK which requires a 16 dB ACR and 32 dB NCR. ACR is the tighter constraint for Butterworth and Chebyshev Type I filters. Instead, Elliptical and Chebyshev Type II filters are limited by the NCR because they have a flat stop-band that must be placed at -32 dB below the pass-band amplitude. Butterworth and Chebyshev Type I filters are then preferred. Unfortunately, Butterworth filters cannot be used for this application since they require a filter order that is simply too large, as it will be possible to see in Table 3.1. However, Chebyshev Type I filters generate a ripple in the pass-band which may corrupt the data transmitted in the channel. Fortunately this ripple is deterministic, so it is possible to compensate the amplitude variation in the digital part of the receiver.

As a side note, another reason to avoid the use of Elliptical and Chebyshev Type II filters comes from the behaviour of the phase of the signal. it is important to control the behaviour of the phase of the signal since QAM stores half of the information on it. The best frequency response of the phase is when it decreases linearly with frequency (in linear scale). This is very convenient because all the phases in the sub-carriers are then subjected to the same relative phase shift. It is easier to obtain this behaviour with Butterworth and Chebyshev Type I filters since they requires only poles in the transfer function. Instead, Elliptical and Chebyshev Type II filters requires both poles and zeros. This makes the behaviour of the phase very difficult to control.

- **Dynamic range:** The receiver must be able to treat incoming signals with a very wide difference in power. The worst case is given by the 802.11n standard, which supports powers from  $-82$  dBm to  $-20$  dBm. Instead, 802.11ac supports powers from  $-82$  dBm to  $-30$  dBm. The equivalent dynamic range is 62 dB for 802.11n and 52 dB for 802.11ac.
- **Linearity (1 dB compression point):** To minimize the noise coming from other frequency signals it is important to have a linear behaviour of the filter for all the possible values of the power of the signal. While the lower end of the dynamic range does not give problems in term of linearity, it is not possible to say the same for signals with larger power. The maximum signal reaches  $-20$  dBm, however it must be considered also the variations of this value. In particular, *OFDM* imposes higher linearity constraints since the sub-carriers can constructively interfere, thus further increasing the signal power. A measure of this phenomenon is given by the Peak-to-Average Ratio (**PAR**), and it depends on the total number  $N$  of active sub-carriers (data plus pilot) [4].

$$PAR = 2 \cdot \ln(N)$$

The number  $N$  depends on the bandwidth. The worst case is found for 160 MHz bandwidth, for a total number of 484 and an equivalent  $PAR = 12.4 = 10.9$  dB. In the end, the filter must remain linear also for larger sig-

nals. The limit is imposed by the 802.11n standard, hence it must have a  $P_{1\text{dB}} = -20 + 10.9 = -9.1$  dBm.

- **Noise figure (NF) and noise floor:** Since each analogue component inject noise in the signal, it is important to know beforehand the tolerance of the standards. It is possible to start the analysis from the definition of the sensitivity in Equation 3.3 [4]:

$$P_{\text{sen|dBm}} = P_{\text{RS|dBm/Hz}} + NF_{\text{dB}} + 10 \log(B) + SNR_{\text{min|dB}} \quad (3.3)$$

Where  $P_{\text{RS}}$  is the source resistance noise power,  $NF$  is the noise figure,  $B$  is the bandwidth of the signal and  $SNR_{\text{min}}$  is the minimum Signal-to-Noise Ratio accepted by the receiver. Considering  $P_{\text{RS}} = k_B \cdot T = -174$  dBm/Hz and rearranging the equation to isolate the noise figure:

$$NF_{\text{dB}} = +174 \text{ dBm/Hz} + P_{\text{sen|dBm}} - 10 \log(B) - SNR_{\text{min|dB}}$$

Table 2.1 provides the  $P_{\text{sen|dBm}}$  while Table 2.4 shows the inverse (negative in dB) of the  $SNR_{\text{min|dB}}$ .

The worst case is found for the combination of 64-QAM modulation and a 5/6 rate, which gives a  $NF = 10$  dB.

It must be noted that the  $NF$  is referred to the whole receiver, so the filter must provide a smaller  $NF$  than the one computed here.

Unfortunately, the  $NF$  is a parameter that can be correctly used only when designing the full analog front-end of the receiver. Then, the noise floor can be used as a parameter in order to estimate the noise requirement. Among the modulations, BPSK is the one which requires the minimum input sensitivity of -82 dBm. Assuming a signal amplification of 30 dB from the LNA and mixer the minimum input sensitivity at the input of the filter becomes -52 dBm. In order to minimize the influence of the filter noise on the signal, a noise floor of maximum half the power of the minimum signal must be generated. It leads to a noise floor of -55 dBm.

### 3.3.1 Towards 802.11ax

The 802.11ax standard must also be taken in consideration in order to conclude the filter analysis. Most of the parameters remains the same, however there is a tighter constraint on the selectivity of the filter. In the following it is presented an update list of all the parameters seen in the previous section.

- **Bandwidth:** 802.11ax supports all the bandwidths already supported by 802.11ac. These are: 20, 40, 80 and 160 MHz
- **Type and order of the filter:** 802.11ax will require more selective filters at the receiver stage. This is due mostly by the occupied bandwidth. In a 20 MHz 802.11ax channel, 245 out of 256 sub-carriers are used. In 802.11ax each sub-carrier has a bandwidth of 78.125 kHz, one fourth of the ones used in 802.11ac. This corresponds to a Transition Band-Width (TBW) of just 0.86 MHz. In the case of 40, 80, 160 MHz channels the TBW is doubled.

Table 3.1 shows the minimum required order for a low-pass filter in order to be compliant with 802.11ax. As a quick remark, the obtained values were found considering the equivalent bandwidth of a low-pass filter, which is half of the band-pass filter required for the aforementioned values.

- **Dynamic range:** In order to support the current standards, the maximum expected dynamic range will be 52 dB, the same as the one required in 802.11ac. The minimum signal power supported by 802.11ax in 1024 QAM will be 6 dB higher than the corresponding value for 256 QAM, the maximum remains equal.
- **Linearity (1 dB compression point):** The maximum expected signal is -30 dB and the peak to average ratio is a bit larger since the maximum number of sub-carriers will be 996. It results in a  $PAR = 13.8 = 11.4$  dB.

The  $P_{1dB}$  must be larger than -18.6 dBm.

- **Noise figure (NF) and noise floor:** The minimum noise figure remains fixed at 10 dB. Also the required noise floor remains the same.

Standard	Filter type	$A_P$ (dB)	TBW (MHz)	BW (MHz)	RFO
802.11ax	Butterworth	1	0.86	10	30 (29.11)
			1.8	20	28 (27.81)
				40	56 (55.66)
				80	112 (111.33)
		2	0.86	10	25 (24.37)
			1.8	20	24 (23.28)
				40	47 (46.60)
				80	94 (93.22)
		3	0.86	10	22 (21.23)
			1.8	20	21 (20.33)
				40	41 (40.70)
				80	82 (81.40)
		4	0.86	10	19 (18.86)
			1.8	20	19 (18.02)
				40	37 (36.05)
				80	73 (72.12)
	Chebyshev Type I	1	0.86	10	8 (7.60)
			1.8	20	8 (7.42)
				40	11 (10.57)
				80	16 (15.01)
2		0.86	10	7 (6.62)	
		1.8	20	7 (6.47)	
			40	10 (9.22)	
			80	14 (13.09)	
3		0.86	10	6 (5.98)	
		1.8	20	6 (5.85)	
			40	9 (8.33)	
			80	12 (11.83)	
4		0.86	10	6 (5.48)	
		1.8	20	6 (5.35)	
	40		8 (7.63)		
	80		11 (10.83)		

Table 3.1: 802.11ax standard Required Filter Order (RFO) for a given Band-Width (BW), pass band attenuation ( $A_P$ ) and Transition Band-Width (TBW).

### 3.4 Required Filter

A filter compliant with the next 802.11ax standard must have high selectivity which translate in a high order. However, the increase of the filter order increases also the number of components or blocks that must be placed in the filter. As a consequence, the power consumption of the filter increases with the order of the filter.

A good compromise between power consumption and selectivity can be achieved with a sixth order Chebyshev Type I filter having a 3 dB ripple in the passband. However, Table 3.1 shows that this configuration can be used only for bandwidths of 10 and 20 MHz. Then, the additional bandwidths of 40 and 80 MHz will not be supported by the proposed filter. This is coherent with the goal of the project since larger bandwidths require both the transmitter and the receiver to consume more power in exchange for an higher throughput. The higher throughput is not always required for devices working in an IoT system.



# Chapter 4

## Base-band filters and source follower state-of-the-art

### 4.1 Introduction

The previous chapters explained the basic notions regarding Radio Transceiver and the standard targeted by this work. This chapter presents now the most common filter topologies used for wireless applications. The main trade-off of these topologies are analysed.

The second part provides an analysis of the state-of-the-art of Source Follower filters, topology of choice for this project. The main characteristics of these filters are presented and compared.

### 4.2 Filter topologies

Active analog filters are a core component in all types of signal processing in a system operating in the analog domain. They are used to select specific frequencies of the signal in order to enhance them or to remove them. The active analog filters can be divided in two large categories: Discrete-time and Continuous-time.

#### 4.2.1 Continuous-time filters

Generally, Continuous-time filters can be composed of both passive and active circuits. Passive circuits are composed of capacitors and inductors connected in series or parallel, they are usually the reference circuits for ideal transfer functions of filters, but they are not considered for baseband implementations since inductors are very large and this translate to a more expensive circuit. In addition, the output signal is always equal or smaller than the input signal. Instead, active circuits contain components which amplify the input signal.

The most used active Continuous-time filters are  $G_m$ - $C$  filters [6] [7] [8] and Active  $RC$  filters [9] [10] [11]. Their frequency response is controlled by the ratio of the  $G_m$  over  $C$  for the former, while it depends by the product of  $R$  and  $C$  for the latter. Typically, Active  $RC$  filters provides higher linearity with respect to  $G_m$ - $C$  ones. However it comes at the cost of larger power consumption and circuit complexity since Active  $RC$  implementation uses a full Op-Amp while a  $G_m$ - $C$  filter uses only an OTA. On the other hand,  $G_m$ - $C$  filters have poor linearity and

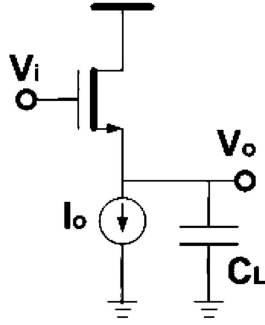


Figure 4.1: First order Low-Pass Filter (LPF) based on source-follower [12]

additional circuitry needs to be added which it often translates in an increased power consumption. Between the two implementations, none comes as a clear winner for the application targeted by this work.

Recently a type of filter based on Source-Follower (SF) architecture has been studied. SF filters have reduced complexity and provide higher linearity with respect to the two implementations described above. On the other side, all aspects of  $G_m$ - $C$  and Active  $RC$  filters have been studied extensively.  $G_m$ - $C$  and Active  $RC$  filters are the de facto standard in IC filter design. Another major drawback is found in the gain of this type of filters. Indeed, the source follower architecture does not provide an amplification of the input signal.

#### 4.2.2 Discrete-time filters

Discrete-time filters work by sampling the input signal, the most important categories are the Switched-capacitor filter (SCF) or the Switched-current filters. These two type of filters have different advantages over Continuous-time filters. They usually have better linearity and better precision in frequency response. The latter feature is especially relevant since the precision depends mainly by the ratio of the capacitance used (easily obtainable on-chip) and by the precision of the reference frequency. In fact, the  $G_m$ ,  $R$  and  $C$  parameters in Continuous-time filters must be tuned properly since their time constant is not well controlled. An excellent ratio of capacitors can be obtained on-chip while the reference frequency can be very precise. However, Discrete-time filters suffer from noise aliasing, charge injection and incomplete settling. In addition, Discrete-time SCF are usually used for frequencies up to few tens of MHz.

### 4.3 Source-Follower (SF) filters

The next chapter will present the proposed configuration from this work. However, in this section it must be first analysed the current state-of-the-art of this type of filters. This section will present only examples of Low-Pass Filter (LPF)

The most simple implementation of a first order LPF is the one shown in Figure 4.1 [12] The ideal transfer function of Figure 4.1 is:

$$H = \frac{1}{1 + sRC} \quad (4.1)$$

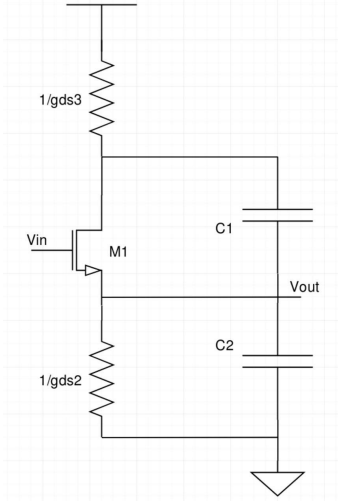


Figure 4.2: second order LPF based on the degenerate source-follower

From this basic circuit block it is possible to build a filter with a second or higher order simply by using many of them in cascade. However it is far more convenient to use the circuit depicted in Figure 4.2. The circuit in Figure 4.2 implements a second order transfer function through a pair of complex-conjugate poles. The transfer function is presented in Equation 4.2.

$$H = \frac{1}{n} \cdot \frac{1}{1 + s \frac{C_1 + C_2}{G_{ms}} + s^2 \frac{C_1 C_2}{g_{ds3} G_{ms}}} \quad (4.2)$$

This configuration has mainly two advantages. Instead of using two blocks as in Figure 4.1 it is now possible to have the same behaviour with only one block, it means that the power consumption is practically halved. The second advantage lies in the amplification loss at the cut-off frequency. In a LPF the cut-off frequency is defined as the frequency at which the output signal amplitude becomes 3 dB lower than the input signal. In the circuit composed by two blocks as in Figure 4.1 the amplitude at the cut-off frequency is attenuated twice by the same amount of 3 dB, resulting in a loss of 6 dB in total. Instead, the circuits in Figure 4.2 has only a loss of 3 dB.

The main categories based on the circuit in Figure 4.2 will be analysed in the next sections. These are the Super SF [13], the Flipped SF [14] and the Cross-coupled SF [12].

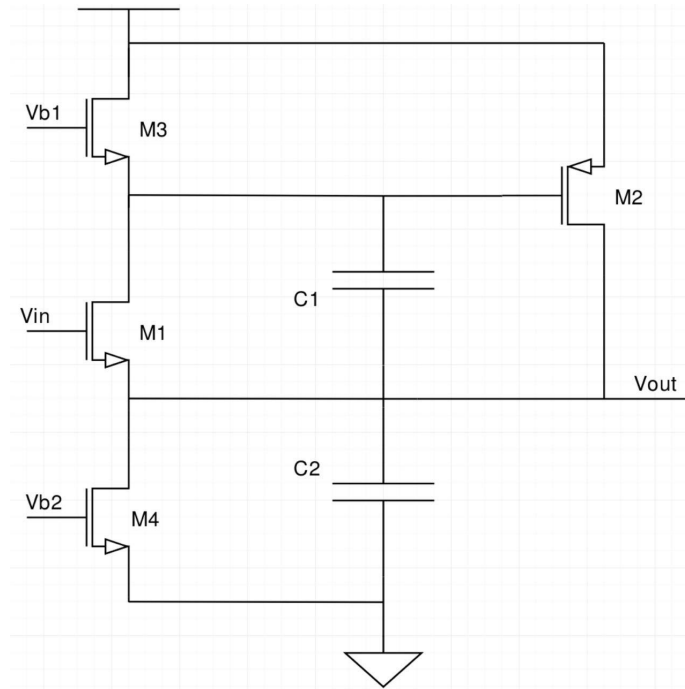


Figure 4.3: second order LPF based on the Super source-follower [13]

### 4.3.1 Super SF

Figure 4.3 shows the diagram of a second order LPF. The main elements in the circuit are transistors M1, M2 and capacitors C1, C2. The other two transistors M3 and M4 provide the biasing current for the system, they do not influence the transfer function as long as they are correctly designed and sized. In fact M3 and M4 are represented just as resistors in the small signal circuit of Figure 4.4. It is possible to retrieve the results resumed in Table 4.1 using the circuit in Figure 4.4. Table 4.1 shows the most relevant parameters from the small signal analysis: DC gain, Quality factor ( $Q$ ), cut-off frequency ( $\omega_0$ ), output impedance ( $Z_{out}$ ), input referred noise resistance ( $R_{n,in}$ ) and the general transfer function ( $H$ ). Note that Table 4.1 shows the approximated computation of these parameters.

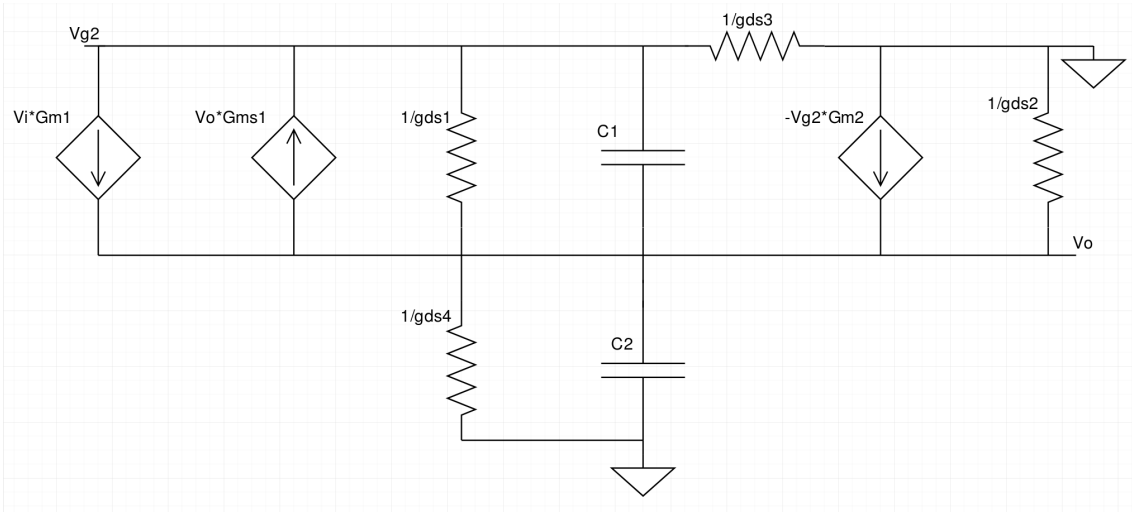


Figure 4.4: small signal analysis for the circuit in Figure 4.3

DC gain	$\frac{1}{n}$
$Q$	$\sqrt{\frac{G_{ms1}C_1}{G_{m2}C_2}}$
$\omega_0$	$\sqrt{\frac{G_{ms1}G_{m2}}{C_1C_2}}$
$Z_{out}$	$\frac{g_{ds1} + g_{ds3}}{G_{ms1}G_{m2}}$
$R_{n,in}$	$\frac{\gamma_{nD1}}{G_{m1}} + \frac{\gamma_{nD2}(g_{ds1} + g_{ds3})^2}{G_{m1}^2G_{m2}}$
$H$	$\frac{1}{n} \cdot \frac{1}{1+s\frac{C_1}{G_{ms1}} + s^2\frac{C_1C_2}{G_{ms1}G_{m2}}}$

Table 4.1: Summary of Super SF filter characteristics

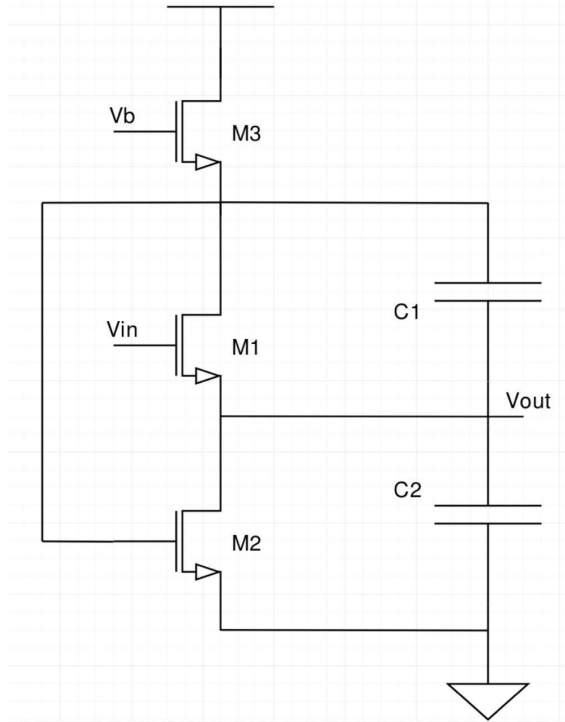


Figure 4.5: second order LPF based on the Flipped source-follower [14]

### 4.3.2 Flipped SF

Figure 4.5 shows the diagram of a second order LPF. The most important components of the circuit are M1, M2, C1 and C2, as in the case of the Super SF. The main difference is that the pMOS (M2) used in the Super SF is now placed as a nMOS. This variation reduce the dimension of the circuit because there is no need for the mirror based on nMOS. The transistor count changes from four, in the case of Super SF, to just three.

In addition, the circuit connections of M2 in the Flipped SF are the same as the ones in the Super SF. That is because the gate of transistor M2 is connected to the drain of M1 for both configurations, the drain of M2 is also connected to the source of M1 and the source of M2 (nMOS in the Flipped SF) is connected equivalently as in the Super SF (pMOS).

The small signal analysis is not different from the Super SF, in fact from Figure 4.6 it is possible to determine that Table 4.1 is valid also for the Flipped SF.

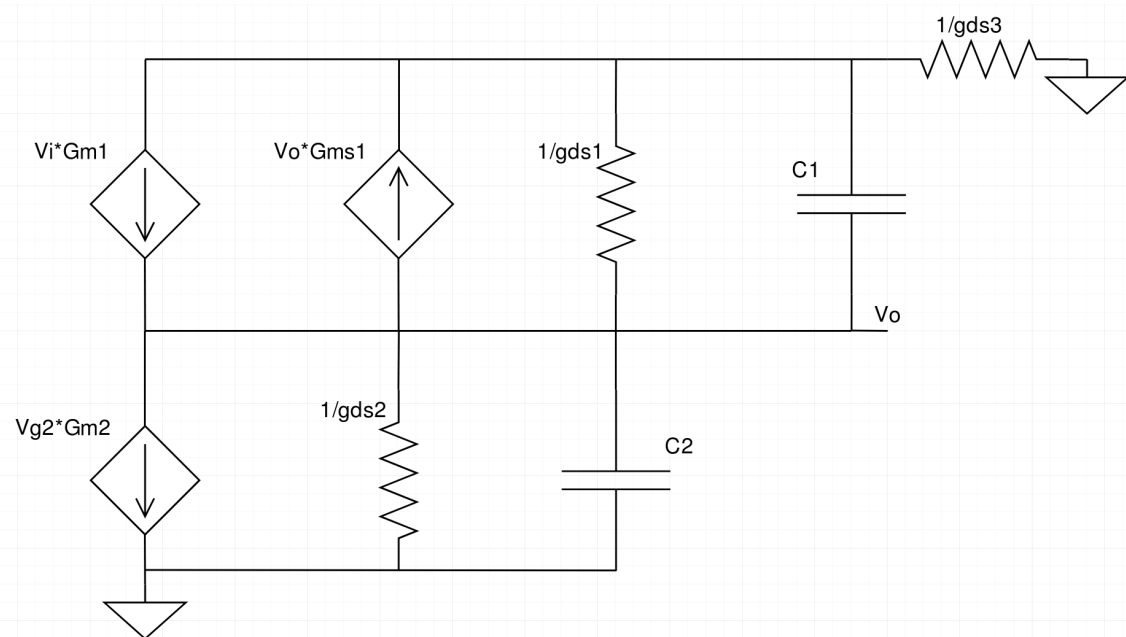


Figure 4.6: small signal analysis for the circuit in Figure 4.5

### 4.3.3 Cross-coupled SF

The last configuration that will be discussed in this chapter is the Cross-coupled SF and Figure 4.7 shows its circuit. This configuration is peculiar with respect to the ones seen in the previous sections because it is a fully-differential circuit while the previous shown circuits are single-ended. Note that also the Super SF and the Flipped SF can be used also in a fully-differential configuration. However it is not possible to use the Cross-coupled SF in a single-ended configuration.

In Figure 4.7 transistors M1 and M4 receive the differential input at their gates. The gate of M2 is connected to the source of M4 while the gate of M3 is connected to the source of M1. Capacitors C1 and C2 are placed across the positive and negative branches so that the required capacitance will be halved with respect to a capacitor connected to ground from one side. It effectively reduces the required capacitances by a factor four.

Table 4.2 shows the most relevant parameters from the small signal analysis. It is possible to notice the similarities between Table 4.1 and Table 4.2. In general, the transfer function and the quality factor of the Cross-coupled SF have more parameters in their equation, which may result in a more complex design phase. Another point that is relevant for the topic of this work is given by the input referred noise. From the two tables it is possible to notice that the Super SF and the Flipped SF have only one component which mainly influences the noise, that is transistor M1 since the relevant term is the one with only  $G_{m1}$  at the denominator. The Cross-coupled SF have instead two terms, coming from M1 ( $G_{m1}$ ) and from M2 ( $G_{m2}$ ) that are equally relevant. Then Figure 4.7 shows a circuit that, from the design standpoint, generate more noise. This can be inconvenient for the application of this work because in analog design an important trade-off is the one between power consumption and noise. Since the targeted design will aim to reduce power consumption it is important to choose the best configuration accordingly.

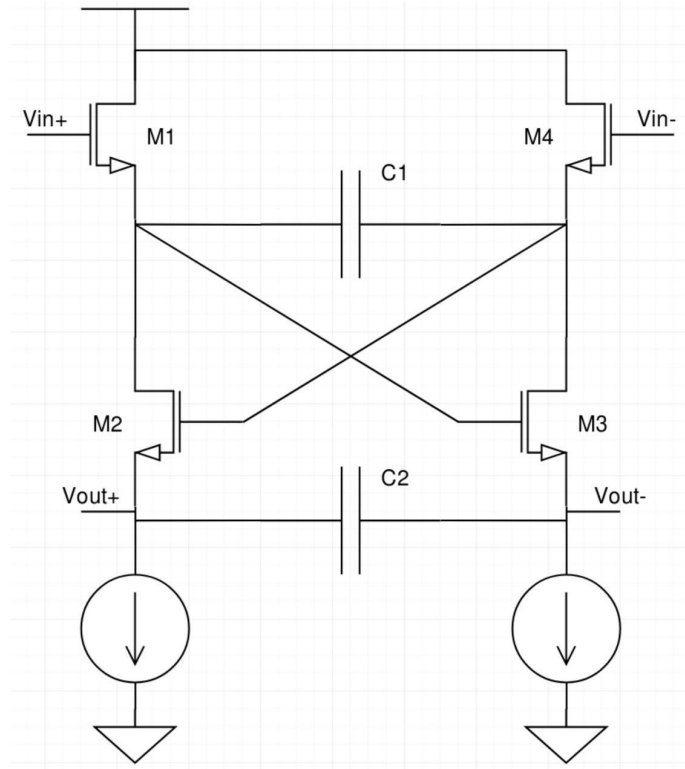


Figure 4.7: second order LPF based on the Flipped source-follower [12]

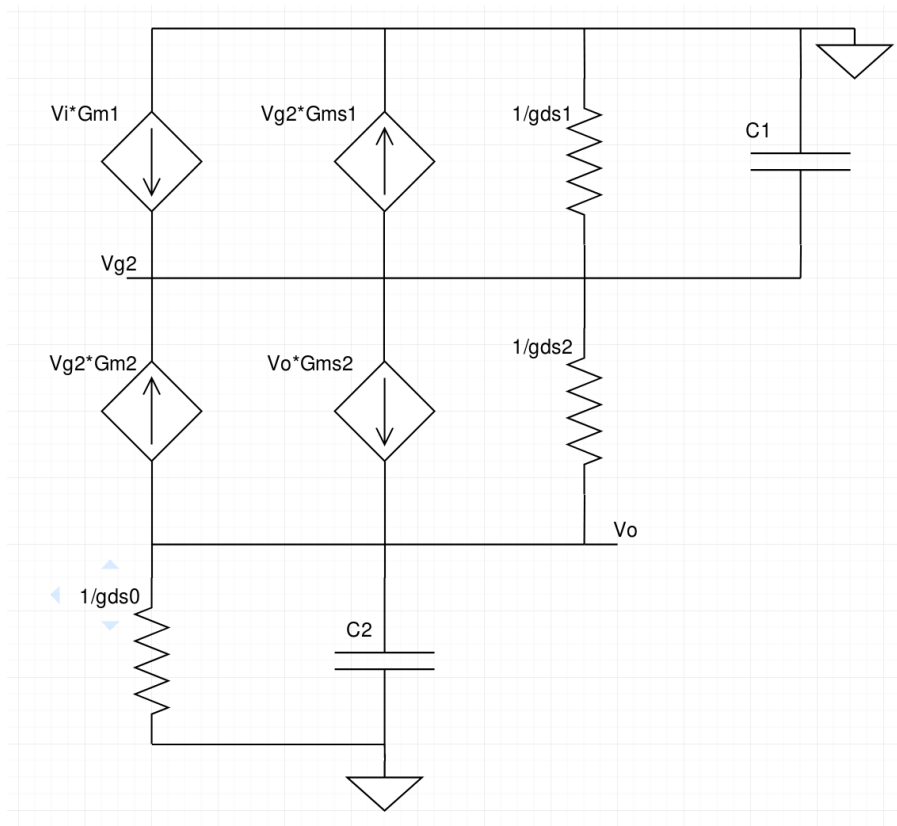


Figure 4.8: differential small signal analysis for the circuit in Figure 4.7

DC gain	$\frac{1}{n}$
$Q$	$\frac{\sqrt{G_{ms1}G_{m2}C_1C_2}}{C_1G_{m2} + C_2(G_{m2} - G_{ms1})}$
$w_0$	$\sqrt{\frac{G_{ms1}G_{m2}}{C_1C_2}}$
$Z_{out}$	$\frac{G_{m2} - G_{ms1}}{G_{ms1}G_{m2}}$
$R_{n,in}$	$\frac{\gamma_{nD1}}{G_{m1}} + \frac{\gamma_{nD2} \cdot n^2}{G_{m2}}$
$H$	$\frac{1}{n} \cdot \frac{1}{1 + s \left[ \frac{C_1}{G_{ms1}} + \frac{C_2(G_{m2} - G_{ms1})}{G_{ms1}G_{m2}} \right] + s^2 \frac{C_1C_2}{G_{ms1}G_{m2}}}$

Table 4.2: Summary of Cross-coupled SF filter characteristics



# Chapter 5

## Proposed configuration

### 5.1 Introduction

This chapter presents the implementation of the sixth order Chebyshev Type I Low-Pass Filter (LPF). The first part explains how to retrieve the ideal transfer function parameters for a second order Chebyshev LPF, which must satisfy the requirements explained in the previous chapters. A sixth order LPF can be built by three second order (biquadratic) filter sub-blocks as explained in the state-of-the-art chapter. The second part analyses the design methodology and the workflow used in this work. The third and last part presents each of these three biquadratic filters and explain their characteristics.

### 5.2 Ideal filter parameters

This section presents in the first part the transfer function of a second order Chebyshev type I filter. The second part shows the transfer function of the ideal complete filter. This filter must match the constraints described in the **IEEE 802.11** standards. In particular, it must be compliant with 802.11n, 802.11ac and 802.11ax.

In general, the LPF transfer function can be written using Formula 5.1 [15]:

$$H = \frac{K}{\prod_{i=1}^N (s - p_i)} \quad (5.1)$$

Where  $K$  is the DC gain,  $N$  is the order of the filter and  $p_i$  are the poles of the transfer function. From the Chebyshev polynomials it is possible to retrieve the values of the poles:

$$p_i = \sigma_i + j\omega_i \quad (5.2)$$

$$\sigma_i = -\omega_p \sinh \left[ \frac{1}{N} \operatorname{arcsinh} \left( \frac{1}{\epsilon} \right) \cdot \sin \left( \frac{\pi}{2N} (2i - 1) \right) \right] \quad (5.3)$$

$$\omega_i = \omega_p \cosh \left[ \frac{1}{N} \operatorname{arcsinh} \left( \frac{1}{\epsilon} \right) \cdot \cos \left( \frac{\pi}{2N} (2i - 1) \right) \right] \quad (5.4)$$

Where  $\omega_p$  is the 3 dB cut-off frequency in the pass band,  $\epsilon$  is a parameter related to the maximum tolerated pass band attenuation  $A_p$ .

$$\epsilon = \sqrt{10^{\frac{A_p}{10}} - 1} \quad (5.5)$$

	$F_r$	$Q$
Cell 1	0.298	1.0442
Cell 2	0.7224	3.4586
Cell 3	0.9771	12.7809

Table 5.1: Values of the quality factor  $Q$  and the cut-off frequency multiplier  $F_r$  for each cell of the final sixth order Chebyshev LPF. They are valid for both 10 MHz and 20 MHz.

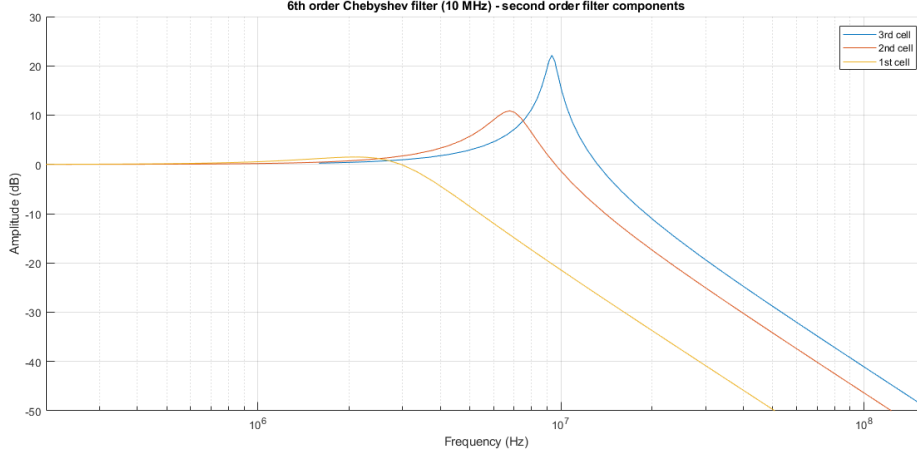


Figure 5.1: The three second order transfer functions required by the sixth order Chebyshev LPF.

### 5.2.1 Parameters values

Using the information summarized in Section 3.4 and considering Equations 5.1 to 5.4 it is possible to retrieve the required parameters for the filter by using Equation 5.6, in which parameter  $K$  is the DC gain,  $Q$  is the quality factor.  $F_r$  multiplies the  $\omega_p$  in order to shift the cut-off frequency.

$$H = \frac{K}{1 + \frac{s}{Q \cdot F_r \cdot \omega_p} + \frac{s^2}{(F_r \cdot \omega_p)^2}} \quad (5.6)$$

$N = 2$  For a biquadratic cell. Choosing  $A_p = 3$  dB leads to an  $\epsilon \simeq 1$  and a  $K = 1/\sqrt{2}$ . The filter must be used for the 802.11 standards, recalling the previous chapters it will require a  $\omega_p = [10, 20]$  MHz. The values of  $Q$  and  $F_r$  depend on the biquadratic cell, Table 5.1 gives the required values.

Figure 5.1 shows the three transfer functions that can be obtained from Table 5.1 and Equation 5.6 for a 10 MHz filter. Figure 5.2 shows the complete filter with also the mask requirements retrieved in Chapter 3.

## 5.3 Filter schematics and small signal models

A biquadratic cell is insufficient to fulfill the specifications in the 802.11ax standard. In fact, 802.11ax will require a very selective LPF. In the case of a Chebyshev Type

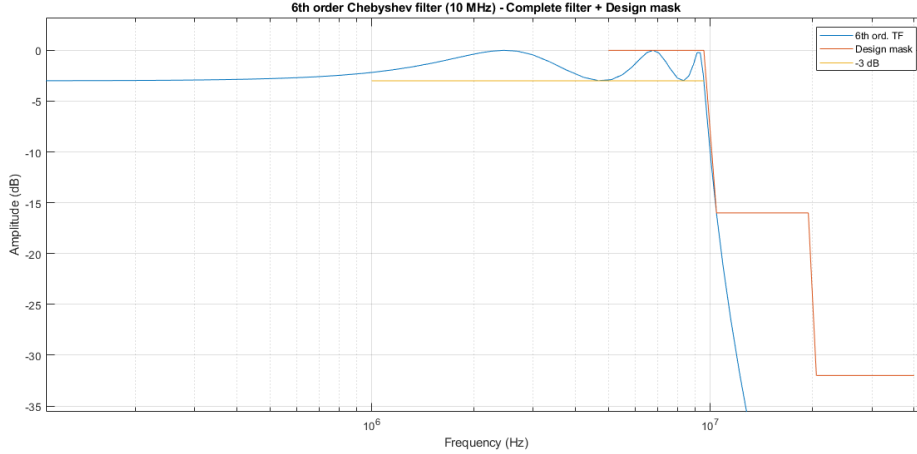


Figure 5.2: Sixth order Chebyshev LPF and Mask requirements.

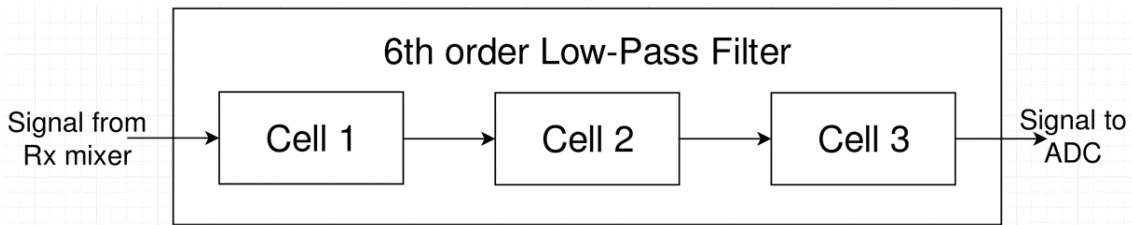


Figure 5.3: General diagram of 6th order Chebyshev LPF.

I filter topology, the minimum required filter order is  $N = 6$ . The general diagram is presented in Figure 5.3.

A sixth order filter is possible by cascading three biquadratic cells, each one implementing a second order filter. To strengthen the signal it is possible to use first an amplifying fully-differential biquadratic cell (1), Figure 5.4 shows the circuit diagram. Then signal passes through two non-amplifying fully-differential biquadratic cells (2 and 3), which have circuit diagrams shown in Figure 5.5 and Figure 5.6.

Figure 5.5 is based on a p-type input MOST while Figure 5.4 and Figure 5.6 have a n-type input MOST. This is necessary in order to stabilize the bias voltage for all the cells. Otherwise, each cell would subtract one  $V_{GS}$  to the following input voltage bias until it is practically impossible to design the next cell.

The amplification of Cell 1 is useful to reduce the noise of the following cells. In addition, it compensates for the little loss in signal strength due to Cell 2 and 3 as expressed in Equation 5.11.

Cell 1 is based on the Flipped SF [14] while Cell 2 and 3 are based on the Super SF [13]. Flipped SF requires smaller area but is more difficult to design due to the operating point of the MOSTs. Conversely, Super SF is simpler to design but requires larger area. The initial implementation of this work had the full filter based on Flipped SF, however a limit on the achievable quality factor of this configuration was discovered. The proposed configuration of Cell 2 and 3 is able to overcome this limitation since it is based on a cascode-aided Super SF. The purpose of the cascode is to better decouple the influence of the components in the  $Q$  formula.

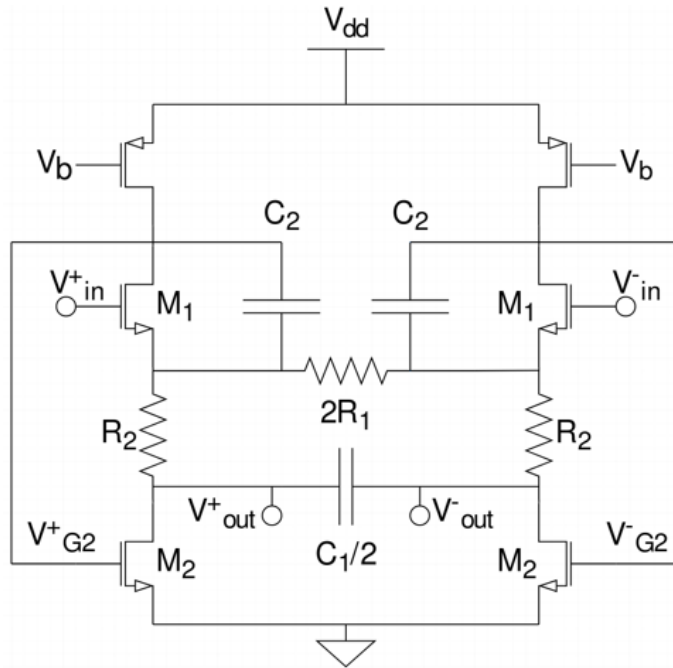


Figure 5.4: Cell 1 - Amplifying fully-differential biquadratic cell based on Flipped SF.

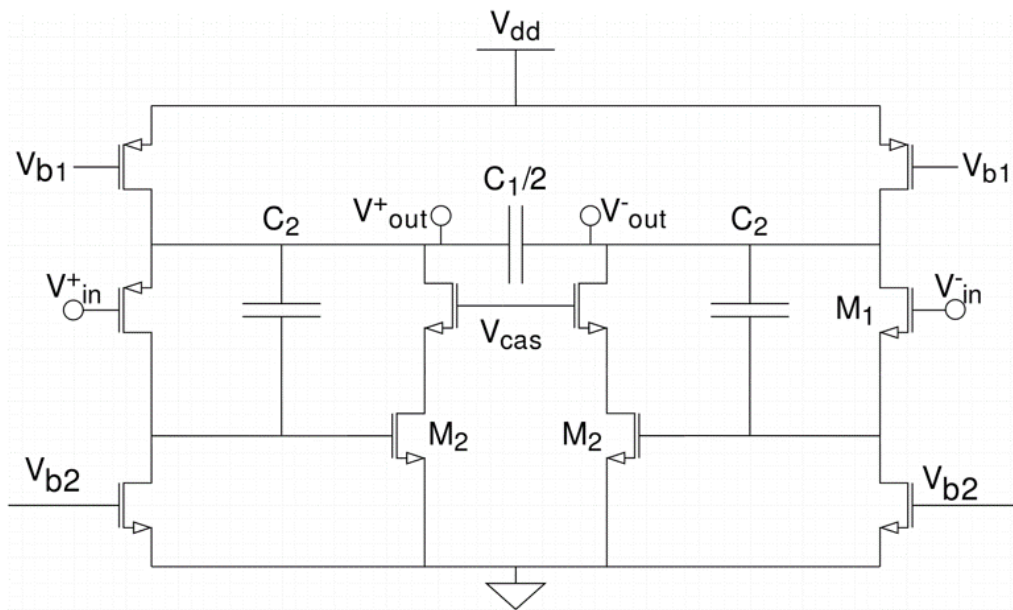


Figure 5.5: Cell 2 - Fully-differential biquadratic cell based on Super SF.

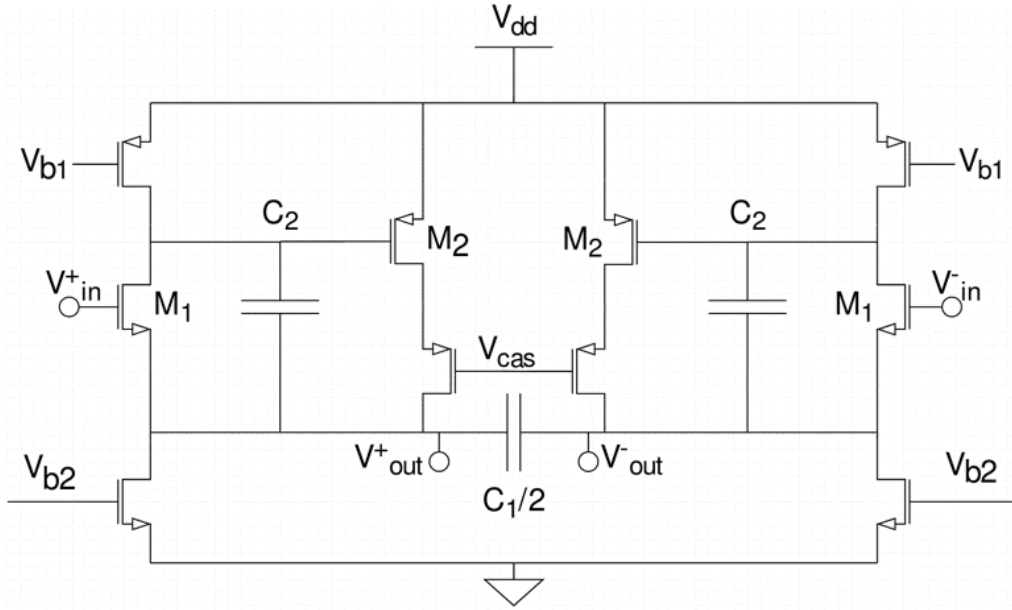


Figure 5.6: Cell 3 - Fully-differential biquadratic cell based on Super SF.

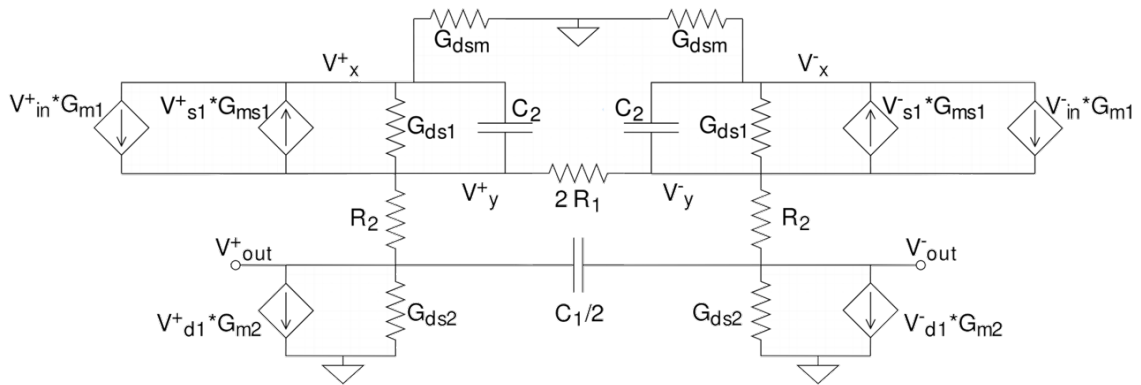


Figure 5.7: Small signal model for Cell 1.

### 5.3.1 Small signal model

The small signal models for Figure 5.4 is presented in Figure 5.7, a common model for Figure 5.5 and Figure 5.6 is presented in Figure 5.8.

From the small signal models it is possible to retrieve the transfer functions of the two biquadratic cells. Equation 5.7 presents the general form of a second order LPF.

$$H_{filter} = \frac{G}{1 + \frac{s}{Q \cdot \omega_c} + \frac{s^2}{\omega_c^2}} \quad (5.7)$$

Where  $\omega_c = F_r \cdot \omega_p$  is the cut-off frequency and  $Q$  is the quality factor of the filter.

In the case of the Cell 1 circuit in Figure 5.7, these three parameters depends on

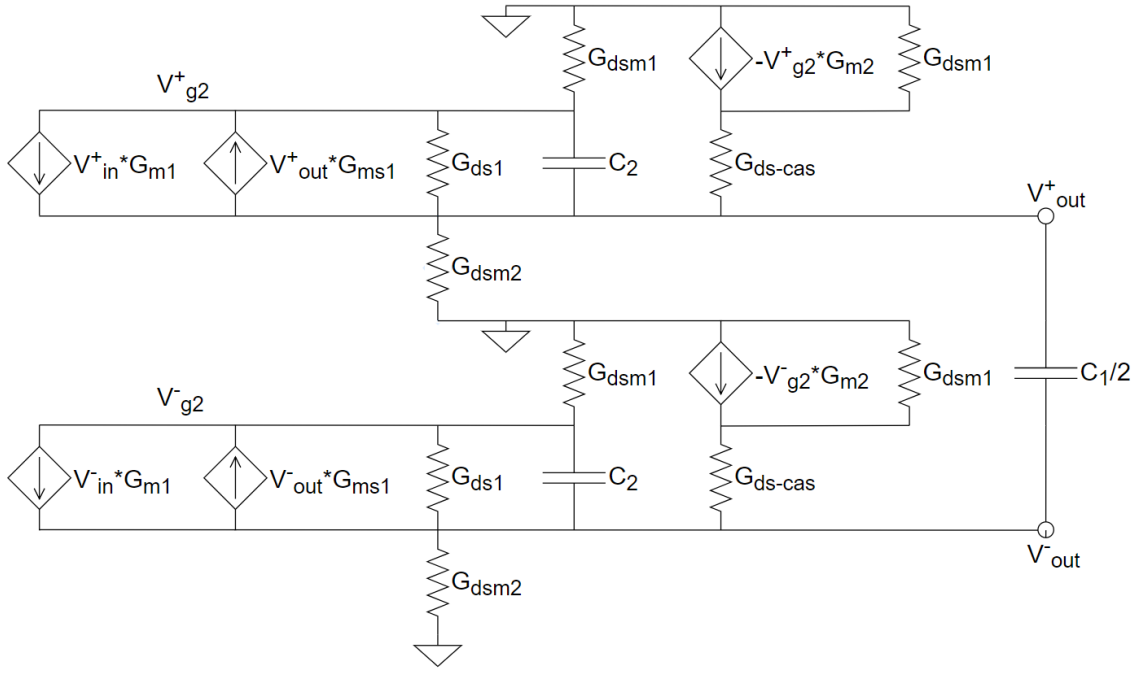


Figure 5.8: Small signal model for Cell 2 and 3.

the following components in a first approximation:

$$G_1 = \frac{1}{n} \left( 1 + \frac{R_2}{R_1} \right) \quad (5.8)$$

$$\omega_{c-1} = \sqrt{\frac{G_{m1}G_{m2}}{C_1C_2G}} \quad (5.9)$$

$$Q_1 = n \sqrt{\frac{C_1G_{m1}G}{C_2G_{m2}}} \quad (5.10)$$

Applying the same small signal analysis to Cell 2 and Cell 3 in Figure 5.8 leads to the following results:

$$G_2 = \frac{1}{n} \quad (5.11)$$

$$\omega_{c-2} = \sqrt{\frac{nG_{m1}G_{m2}}{C_1C_2}} \quad (5.12)$$

$$Q_2 = \sqrt{\frac{nG_{m1}C_1}{G_{m2}C_2}} \quad (5.13)$$

To complete the small signal analysis it is presented also the expressions of the output impedance and the input-referred noise, considering the latter as an equivalent resistance placed at the inputs of the biquadratic cells.

$$Z_{out-1} = \frac{g_{ds1}G}{G_{m1}G_{m2}} \quad (5.14)$$

$$R_{n,in-1} = 2 \left( \frac{\gamma_{nD1}}{G_{m1}} + \left( \frac{g_{ds1}^2}{G_{m1}^2G_{m2}} \right) \gamma_{nD2} + \frac{R_2}{G^2} + 2n^2R_1 \right) \quad (5.15)$$

$$Z_{out-2} = \frac{g_{ds1} + g_{dsm1}}{nG_{m1}G_{m2}} \quad (5.16)$$

$$R_{n,in-2} = 2 \left( \frac{\gamma_{nD1}}{G_{m1}} + \frac{(g_{ds1} + g_{dsm1})^2}{G_{m1}^2 G_{m2}} \gamma_{nD2} \right) \quad (5.17)$$

### 5.3.2 Design challenges

During the design stage it is important to balance the required parameters in order to obtain the wanted behaviour from the analog circuit. Among the three cells, special care must be taken for Cell 1. In fact, the obtained signal amplification further reduces the design space. According to the required parameters there are different options:

- **Power:** Power consumption in analog circuits depends on  $V_{DD}$  voltage and bias current. In the 28 nm node technology the voltage is fixed at 0.9 V. The only option to decrease power consumption is to reduce the bias current which translate in a reduction of the transistors  $G_m$ .
- **Noise:** As seen in Equation 5.15, Noise depends mainly from M1 and  $R_1$ . Noise reduction can be achieved by decreasing their contribution. The most useful options are to increase  $G_{m1}$  and to reduce  $R_1$ . It can be be also possible to further reduce the noise by increase the gain  $G$ .
- **Area:** The smaller the area of the circuit the cheaper it is. For the same current, the lower the  $IC$  of a transistor the wider it needs to be. However, the most effective option to reduce area is to reduce the size of capacitors,  $C_1$  and  $C_2$ , placed in the system.
- **Gain:** In order to increase the gain of the cell the two straightforward options obtained from Equation 5.8 are to increase  $R_2$  or to decrease  $R_1$ .
- **Bandwidth:** Equation 5.9 shows that the bandwidth depends on the product of the two  $G_m$  over the product of the two  $C$  times the gain  $G$ . The best way to tune the cut-off frequency is to fix the gain beforehand and to compute the required values for the other parameters.
- **Quality factor:** Equation 5.10 shows that the quality factor depends on the ratio  $C_1/C_2$  times the ratio  $G_{m1}/G_{m2}$  times  $G$ . As already said for the bandwidth, it is better to fix the gain beforehand and to compute the required values for the other parameters.
- **Dynamic Range:** Cell 1 is the bottleneck of the filter when it comes to dynamic range. This is because Cell 1 has  $R_1$  which lets current flow from the positive branch of the cell to the negative or vice versa. In the case of small signal this is not an issue because the voltage across  $R_1$  is small and there is enough current for the circuit to work linearly. However, the circuit start to behave non-linearly when the current  $I_{R1} = V_{R1}/R1$  flowing in  $R_1$  becomes comparable with the bias current. The stronger the voltage across  $R_1$  the stronger the non-linearity. Once  $I_{R1}$  is almost equal to  $I_D$  there is no

more current to maintain the saturation of M2 in one of the two branches. This results in a clipping phenomenon at the output of the cell.

The most effective options to reduce this problem are to increase the bias current or to increase resistance  $R_1$  and to reduce the gain.

Another requirement that must be satisfied is the saturation condition on transistor M2. The condition of saturation requires the voltage at the drain of M2 to be larger than the saturation voltage:  $V_{D2} > V_{Dsat2}$ , where  $V_{Dsat2} = (V_{G2} - V_{th-2})/n = (V_{D1} - V_{th-2})/n$ . From the circuit perspective, this also requires that  $+V_{DSm} + V_{DS1} + V_{R2} + V_{DS2} < V_{DD}$ , where  $V_{DD} = 0.9V$  is the supply voltage,  $V_{DSm}$  is the drain to source voltage of the p-MOS current mirror,  $V_{R2}$  is the voltage across resistance  $R_2$ ,  $V_{DS1}$  and  $V_{DS2}$  are the drain to source voltage of transistor M1 and M2. From the design perspective is also important that  $V_{G1} = V_{GS1} + V_{R2} + V_{DS2} < V_{DD}$ . Here  $V_{G1}$  is the gate voltage and  $V_{GS1}$  is the gate to source voltage of M1.

The saturation condition in Cell 2 and Cell 3 is not so difficult to achieve since these cells are based on the Super SF architecture. Also, the lack of resistors further improves the design space of the two cells.

### 5.3.3 Quality factor

The standard configuration of the Super SF shows some limitation when trying to achieve high quality factor. In fact, during the design phase it was not possible to achieve  $Q$  larger than 6-7. This is a problem since Table 5.1 requires Cell 3 to achieve a  $Q$  higher than 12. The limitation is easily explained when analysing again the expression of the  $Q$  from the small signal analysis. For high quality factor Equation 5.13 must be substituted with the more accurate Equation 5.18 presented below.

$$Q_2 = \frac{\sqrt{nG_{m1}G_{m2}C_1C_2}}{G_{m2}C_2 + G_{ds1}C_1} \quad (5.18)$$

Equation 5.18 holds because high  $Q$  requires to greatly increase both  $G_{m1}/G_{m2}$  and  $C_1/C_2$ . It means that  $G_{m1}$  and  $C_1$  are much larger than  $G_{m2}$  and  $C_2$ . Unfortunately, also the output conductance  $G_{ds1}$  increases when  $G_{m1}$  does. At the end, the dominant component at the denominator of Equation 5.18 becomes  $G_{ds1}C_1$  even though  $G_{ds1}$  is much smaller than  $G_{m2}$ .

The cascode-aided Super SF was designed in order to decouple the quality factor from the term  $G_{ds1}C_1$ . Equation 5.19 shows that  $G_{ds1}$  is always present but it is not multiplied by  $C_1$  anymore.

$$Q_{2-cas} = \sqrt{\frac{nG_{m1}C_1}{G_{m2}C_2 \left(1 + \frac{G_{ds1}}{G_{ds-cas}}\right)}} \quad (5.19)$$

## 5.4 Model and workflow

The EKV model is used in this work in order to target low power application. This model is particularly useful because it models very well the behaviour of MOSTs in moderate and weak inversion. In addition, with the latest technology nodes these

regions tend to be preferred. In fact, the supply voltage needs to be decreased when moving from a larger technology node to a smaller one while the threshold voltage of MOSTs does not scale very well with technology. In the end, the operative point of MOSTs is getting closer to these regions [16].

The EKV model introduces the Inversion Coefficient ( $IC$ ), presented here in Equation 5.20, where  $I_D$  is the drain current.

$$IC = \frac{I_D}{2n\mu C_{ox} \frac{W}{L} U_T^2} \quad (5.20)$$

This parameter is used to tell the inversion level of a particular MOST:

- For values larger than 10 the MOST is in strong inversion.
- For values smaller than 0.1 the MOST is in weak inversion.
- For values between 0.1 and 10 the MOST is in moderate inversion.

Other useful formulas in the design are presented in Equation 5.21 5.22 5.23.

$$\frac{W}{L} = \frac{I_D}{I_S IC} \quad , \quad I_S = 2n\mu C_{ox} U_T^2 \quad (5.21)$$

$$\frac{G_m n U_T}{I_D} = \frac{\sqrt{(1 + \lambda_c \cdot IC)^2 + 4IC} - 1}{IC(\lambda_c(\lambda_c IC + 1) + 2)} \quad , \quad \lambda_c = \frac{L_{sat}}{L} \quad (5.22)$$

$$\frac{V_G - V_{th} - nV_S}{nU_T} = \ln(q_s) + 2q_s \quad , \quad q_s = \frac{1}{2} \left( \sqrt{(1 + \lambda_c \cdot IC)^2 + 4IC} - 1 \right) \quad (5.23)$$

The EKV model requires only four technology parameter to be known: the specific current  $I_S$ , the fraction of the channel under velocity saturation  $\lambda_c$ , the threshold voltage  $V_{th}$  and  $n$ .

### 5.4.1 Design methodology

This part presents the method used to design the LPF taking advantage of the equations presented in the previous section. Figure 5.9 shows the general workflow for the first cell. The second and third cell can refer to this model even though their configuration is different and easier to design.

Starting from the noise limitation it is possible to set a minimum on the value of the transconductance  $G_m$  and a maximum for the values of the resistors. The trade-off between noise and power is a well known limitation when it comes to analog circuits design. More noise must be generated in order to decrease power consumption. The minimum signal required for the 1024 QAM of the 802.11ax standard is -53 dBm. It is important to generate a noise floor lower than this value so that the noise of the filter will not alter significantly the signal coming from other blocks. From the constraints in the cut-off frequency and quality factor presented in Table 5.1, and selecting a value for  $G_{m2}$  it is possible to retrieve the values for  $C_1$  and  $C_2$ . Imposing the  $V_{GS2}$  allows to fix the operating point of transistor  $M_2$  and its Inversion Coefficient. The bias current for each branch  $I_D$  can be retrieved. As a consequence, the  $W/L$  of the MOSTs are finally defined. Appendix A shows an example of design using Matlab.

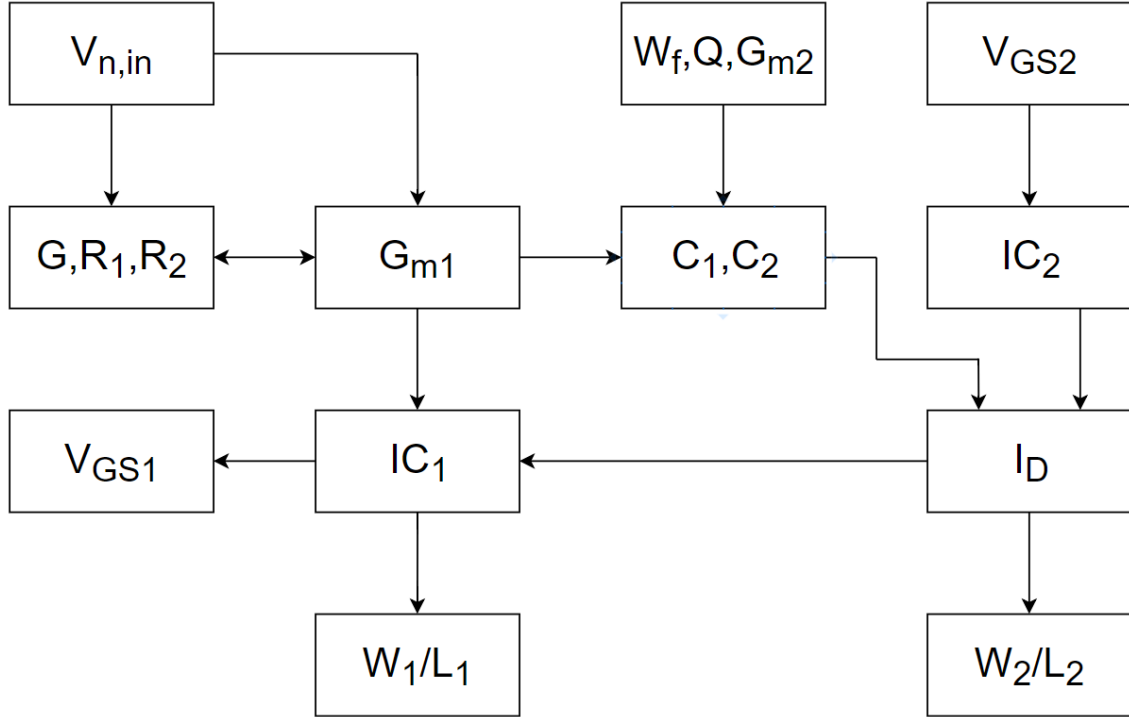


Figure 5.9: Workflow used to size the first cell.

## 5.5 Filter sizing - 10 MHz

This section provides the dimensions chosen for the components of the filter. Given the specification in Table 5.1 and the conditions provided in the previous sections, Table 5.2 presents the sizing for all the components of the cells. For all the cells was chosen a  $L = 500$  nm in order to reduce the contribution of the output conductance on the transfer function of the filter. The voltage applied to the gates of the cascode transistors is  $V_{cas} = 0.15V$  for Cell 2 and  $V_{cas} = 0.7V$  for Cell 3.

Cell	$R_1$	$R_2$	$C_1$	$C_2$	$G_{m1}$	$G_{m2}$	$W_1$	$W_2$	$I_D$
1	$5.8k\Omega$	$5.8k\Omega$	12.8pF	8.8pF	$300\mu S$	$150\mu S$	$16\mu m$	$3\mu m$	$8\mu A$
2	-	-	4.6pF	1pF	$300\mu S$	$100\mu S$	$64\mu m$	$3\mu m$	$10.5\mu A$
3	-	-	2.8pF	0.8pF	$400\mu S$	$100\mu S$	$48\mu m$	$1\mu m$	$8\mu A$

Table 5.2: Values of all the components in Cell 1, 2 and 3 for a cut-off frequency of 10 MHz.

### 5.5.1 From 10 to 20 MHz

In order to switch from 10 MHz cut-off frequency to 20 MHz it is required to change few parameters. Cell 2 and Cell 3 have the advantage to easily shift their cut-off frequency by tuning only their bias current without affecting the quality factor of the transfer function. The same cannot be said for Cell 1 since a change in bias current will completely change the operating points of transistors M1 and M2. Table 5.3 shows the parameters that must be changed from Table 5.2 in order to shift the

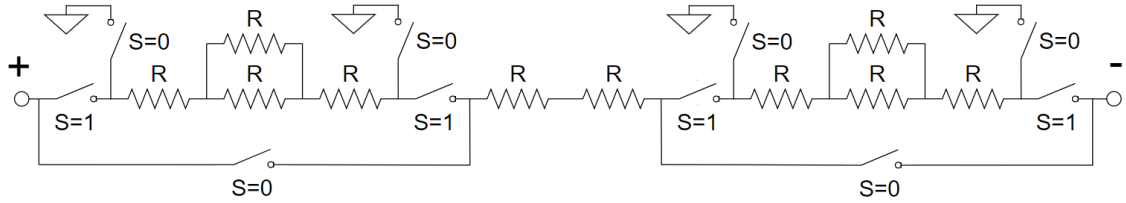


Figure 5.10: Implementation of resistor  $R_1$ , where  $R = 825 \Omega$ .

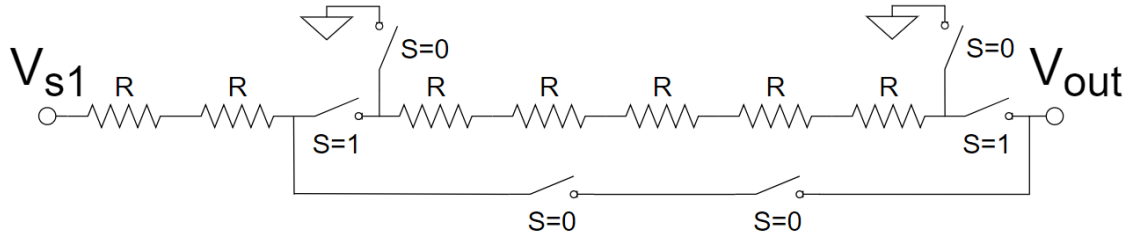


Figure 5.11: Implementation of resistor  $R_2$ , where  $R = 825 \Omega$ .

filter bandwidth from 10 MHz to 20 MHz. The remaining parameters in Table 5.2 must be kept constant.

Cell	Parameter	Value @ 10 MHz	Value @ 20 MHz
1	$I_D$	8 $\mu\text{A}$	24 $\mu\text{A}$
	$R_1, R_2$	5.8 k $\Omega$	1.65 k $\Omega$
	$C_1$	12.8 pF	19.2 pF
	$C_2$	8.8 pF	5.6 pF
2	$I_D$	10.5 $\mu\text{A}$	26 $\mu\text{A}$
3	$I_D$	8 $\mu\text{A}$	17 $\mu\text{A}$

Table 5.3: Required variation in parameters for cut-off frequency of 10 MHz and 20 MHz.

Current  $I_D$  is provided by an external current source so it will not be a concern in this work. Resistors  $R_1, R_2$  and capacitors  $C_1, C_2$  must change their values depending on the considered frequency. These changes are implemented through transmission gates that acts as digital switches in the circuit. Figure shows the schematic implementation of resistors  $R_1$  and  $R_2$ . Additional switches are placed to keep  $R_1 = R_2$  in every case, it must be noted that real switches have an on resistance which must be taken in account. Furthermore, when some of the resistors are not used they are shorted to ground in order to avoid floating voltages.

The capacitor implementation is simpler with respect to the resistances since there is no need to short some connection to ground or to compensate for the on resistance of the transmission gate.

In order to simplify the design stage, all the digital switches are connected in such a way that they are driven by only one external digital signal. Then, in order to change the bandwidth of the filter only a digital signal and the currents of the filter are required to change.



# Chapter 6

## Layout design

### 6.1 Introduction

The first part explains some of the basic layout rules that the designer should follow to reduce mismatches and parasitic capacitances. The second part focuses on the layout of the filter starting from each single cell and concluding with the full filter layout.

### 6.2 Layout rules

Good analog design requires several years of experience because there are a lot of aspects to consider. The higher the frequency of the signal, the more difficult it is for the designer to implement a good layout. For instance, Radio Frequency (RF) layout usually consider frequencies in the range of GHz and it is very easily influenced by the choices of the designer in the layout. This work needs to consider frequencies that are much lower than RF, in the order of few tens of MHz.

One of the most important aspects to consider is to make the circuit independent from absolute value parameters. The general design aims to build a circuit composed of ratio of values because their variation is much smaller than absolute value one. Variation in ratio of values is also called mismatch.

In order to minimize mismatches there are eight basic matching rules [17]:

1. **Identical structure:** The technology parameters depends on the structure of the components and on the layers used to connect them.
2. **Identical temperature:** Many electrical parameters depends on the temperature of the silicon chip. In order to reduce the difference of temperature between two components it is important to place them close to each other and, if possible, far from the heat source. In addition it is better to place the components according to an axis of symmetry for the heat source so that the components will lay in a region at the same temperature.
3. **Same shape and size:** In addition to point 1, there are uncertainties in fabrication processes that limits the reliability of the layout. The same shape and the same size must be ensured in order to obtain the designed values.

4. **Minimum distance:** Parameters such as resistivity and dielectric constant varies from region to region on the chip. Then, it is important to place the matched components as close as possible.
5. **Common centroid geometry:** It is a very effective technique used to minimize mismatches in MOSFETs. The transistors are divided in multiple fingers. In case of two transistor: the fingers of the first transistor are placed among the fingers of the second one so that any variation on the chip affects equally the two components. The complexity of the common centroid increases with the number of transistor to be matched and by the wanted geometry.
6. **Same orientation:** The anisotropy of the silicon can cause systematic mismatches, i.e. in the threshold voltage.
7. **Same surroundings:** Components, especially transistors, placed at the center of the circuit have different surroundings with respect to the ones placed at the edges. To compensate for this difference, it is usual to add few inactive (dummy) components at the sides of the active ones.
8. **Non-minimum size:** It can be shown that the mismatch is inversely proportional to the area of the components.

Another important part of the layout is routing the components. The poly-silicon used to connect the gates of MOSTs is not ideal for the connection different fingers due to the high resistivity of this material. The preferred choice is to use different layers of metal lines. The layers closer to the active region have smaller number. Metal 1 and 2 are used in order to rout the different fingers of the transistors, Metal 3 is also used in case a more complex common-centroid structure requires additional connections. Metal 2 to metal 5 are used to connect different transistor blocks, metal 2 and 4 are used for horizontal connections while metal 3 and 5 are used for vertical ones. Metal 1 is the preferred layer for ground connections while metal 8 is used for  $V_{DD}$ .

It is also important to consider the width of metal lines and VIAs. A general rule tells that each micrometer of metal width can carry up to 1 mA of current. This proportion can vary from one technology node to another so the presented layout doubles this proportion, so that two micrometers are required to carry 1 mA of current.

The layout uses components from the 28 nm technology library provided by TSMC: *rupolym* for the required resistors, *cfmom\_2t* for capacitors, *nch\_ulvt\_mac* and *pch\_ulvt\_mac* for n-MOST and p-MOST respectively.

It must be noted that the whole filter is designed considering a vertical axis of symmetry.

## 6.3 Layout implementation

Following the sequence presented in the previous chapter, this section will present the layout of each cell. For each cell no capacitors are added for better clarity. Then, the full filter layout is presented. As a remark, a 28 nm technology node provided by TSMC has been used.

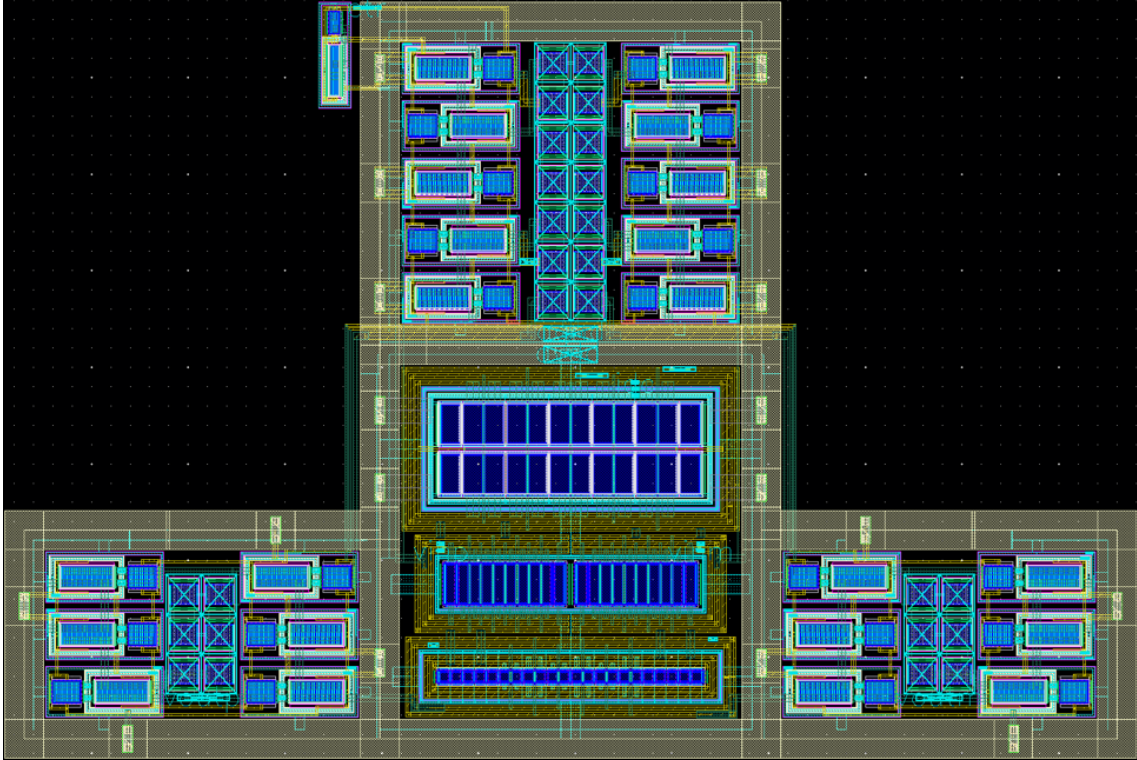


Figure 6.1: Layout of the first cell without capacitors, transistors at the bottom part of the centre, system of resistances at the sides and at top part of the centre.

### 6.3.1 Cell 1

Figure 6.1 presents the layout of Cell 1. Figure 6.1 can be divided in four parts. At the bottom part of the centre are placed all the transistors, while the top part is composed of the circuit implementing  $R_1$ . The other two parts at the sides consist of the circuits for the resistance  $R_2$ , one at the right for the positive branch and another at the left for the negative one.

Common centroid structure is used for p-MOSTs of the current mirror and for n-MOSTs in M2. It is not possible to use common centroid geometry for M1 since the two branches do not have a common source. The only option to reduce mismatches is to place the two transistors M1 as close as possible.

The routing method of this cell follows the standard procedure learned during previous classes at EPFL. The transistors are encircled by many concentric lines of metal 2, one for each required contact. Drain, Gate and Source of all the transistors are then connected through lines of metal 3. Metal 1 is reserved for power connections,  $V_{DD}$  or ground.

Big resistors are placed in order to reduce mismatches. Transmission gates are placed at the sides of resistors in order to change digitally the resistors value. Transmission gates are designed with large  $W$  and minimum  $L$  (30 nm) in order to minimize their on resistance  $R_{on}$ . Also an inverter is placed in the top-left corner in order to generate both positive and negative signals to correctly drive the two transistors in the transmission gate configuration.

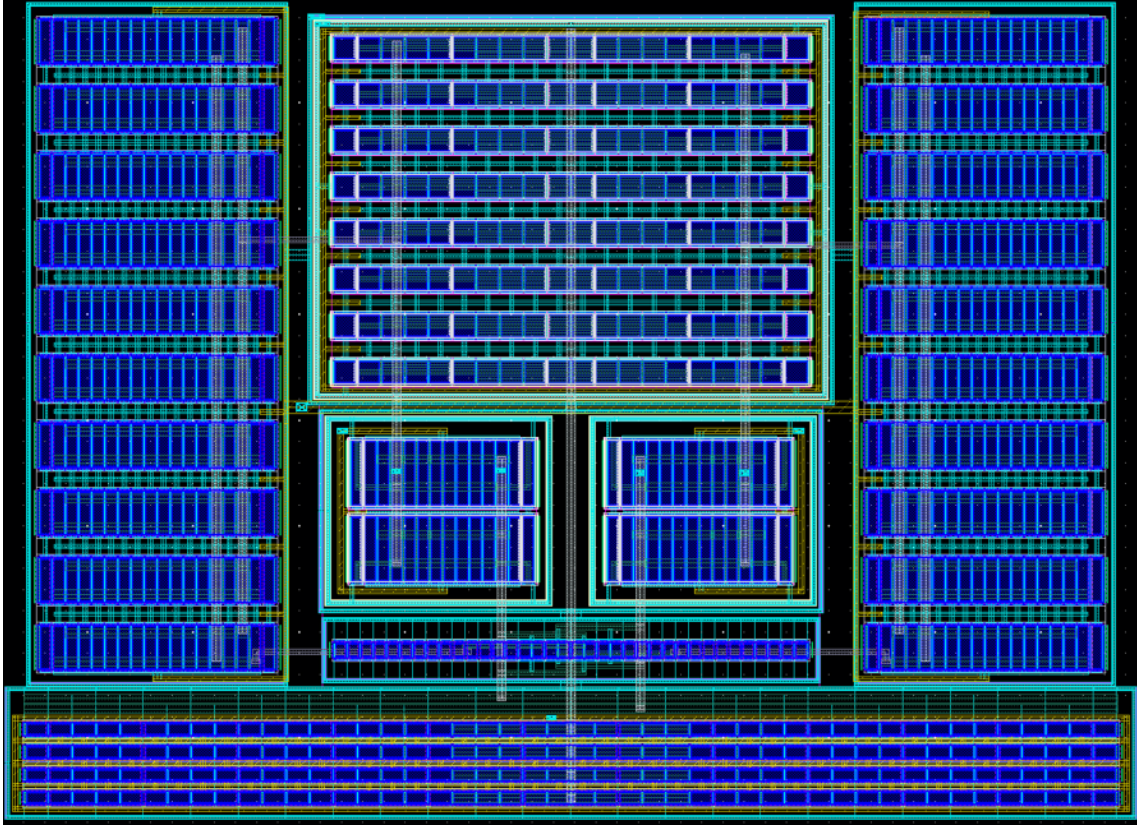


Figure 6.2: Layout of the second cell without capacitors.

### 6.3.2 Cell 2 and 3

Figure 6.2 and Figure 6.3 present respectively the layout of Cell 1 and Cell 2. As already seen in the previous chapter, the circuit of two cells is identical. The only differences between the two cells are the swap of n/p-MOSTs with p/n-MOSTs and the actual sizes of the components.

Only Figure 6.2 is taken in consideration keeping in mind that Figure 6.3 is the same as Figure 6.2 with the difference on the size of the transistors. Figure 6.2 is constituted by six well visible blocks of transistors. The bottom is occupied by the second current mirror. The two sides are occupied by the large cascode transistors. The centre region is occupied, from top to bottom, by the first current mirror, M1 transistors and then also the ones of M2.

Common centroid geometry is used for all blocks excepts for M1 and the transistors of the cascode.

Cell 2 and Cell 3 have a different type of routing with respect to Cell 1. This different method uses the region above the active part of the transistors in order to rout their Drain and Source, usually with metal 3. This approach is usually used in RF designs because it adds less capacitances from the metal layers interconnections and also because it makes the layout overall more compact. The Drain and Source are connected through VIAs that directly connect the metal 3 with the contacts. Metal 2 is usually used for the Gate connections while metal 1 is reserved for  $V_{DD}$  and ground. Metal 4 and metal 5 are used to interconnect the different blocks of the cell.

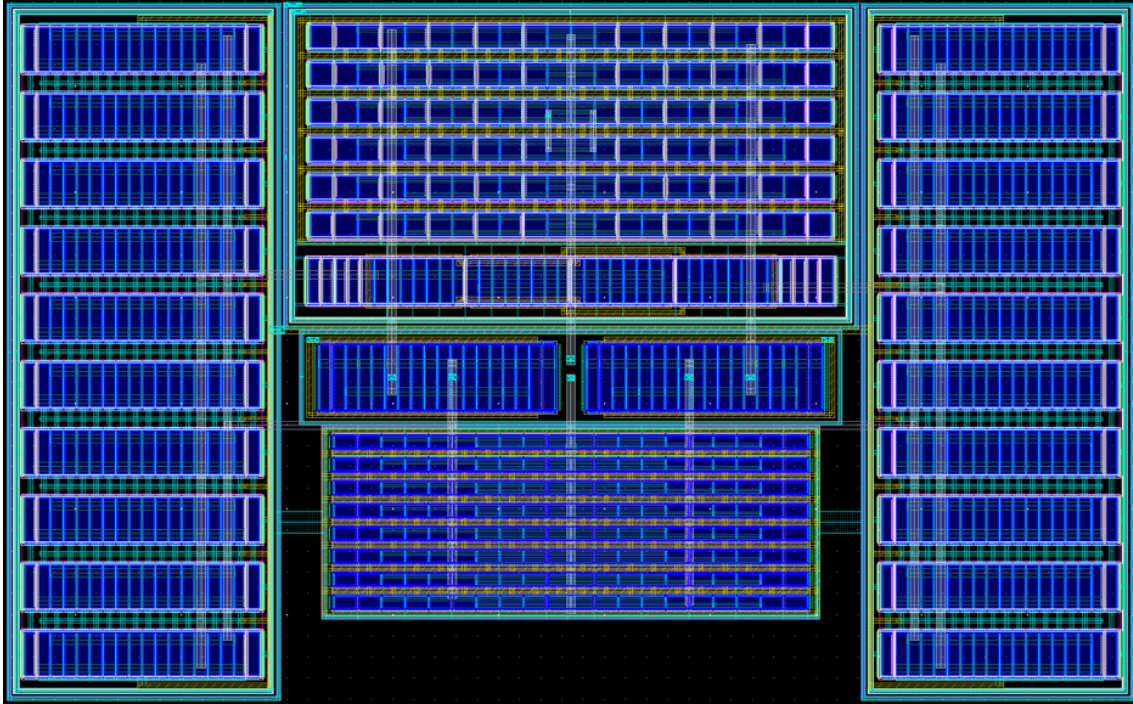


Figure 6.3: Layout of the third cell without capacitors.

### 6.3.3 Complete layout

Figure 6.4 presents the entire filter layout. For routing purpose, Cell 2 is horizontally flipped with respect to the layout presented in Figure 6.2.

Also, capacitances are placed all around the three cells. A small capacitive unit of 200 fF is placed as the basic component of  $C_1$  and  $C_2$  of the three cells. All the capacitors required by Table 5.2 are formed by multiples of this unit connected in parallel. On the top part it is possible to notice also the switches used for changing the capacitors of Cell 1. Another additional inverter is placed in the top part just for maintaining the filter symmetry. Unfortunately, the filter is not entirely symmetrical due to the capacitor switches of Cell 1. In fact, part of the capacitance is shared between  $C_1$  and  $C_2$  of the negative branch of the filter. This is feasible because the value of  $C_1$  increases with the cut-off frequency, while  $C_2$  decreases for the same conditions. However, The total Cell 1 capacitance  $C_1 + C_2$  is different for 10 MHz and 20 MHz which makes it impossible to have both  $C_2$ s to share capacitance with  $C_1$ .

Note also that there are few capacitance in the lowest part of the layout that are more spread out with respect to the rest. These capacitances are the ones used in the third stage. Cell 3 has the highest  $Q$  which means that it is easier to influence it in the layout design. The choice to spread out the capacitances is to allow larger metal contacts to and from the transistors region.

In total the circuit has a Width of 100  $\mu\text{m}$  and a Height of 150  $\mu\text{m}$

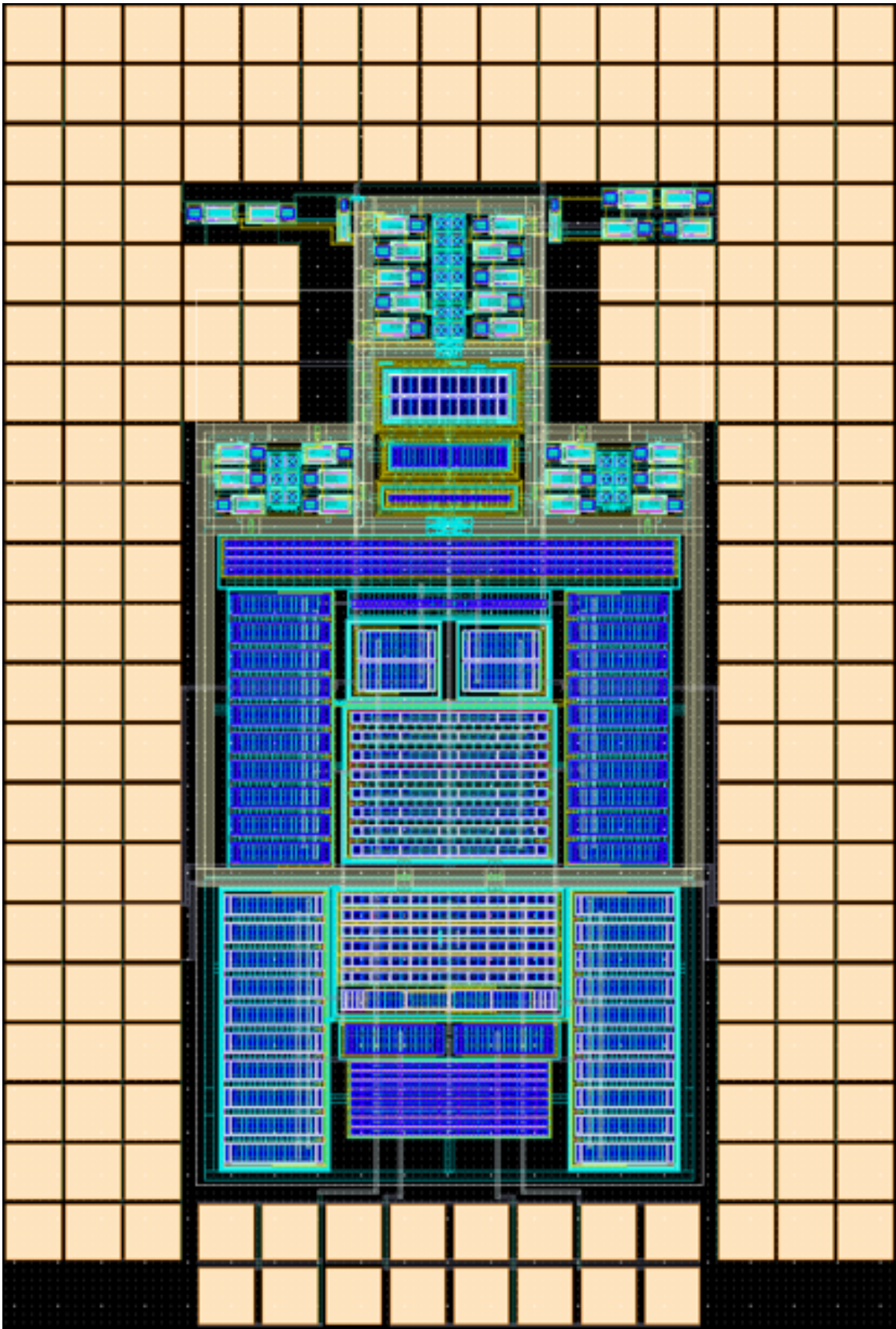


Figure 6.4: Complete layout of the sixth order LPF



# Chapter 7

## Results

### 7.1 Introduction

This chapter presents the results of the simulations performed on the filter after the layout presented in Chapter 6. Once the post-layout results are available, it is possible to check if the circuit is compliant with the requirements. This chapter also presents a comparison with the state-of-the-art of the most relevant parameters in filter design. In addition a Figure-of-Merit (FoM) is introduced in order to evaluate the overall performances of this work.

### 7.2 Post-layout results

This section presents the post layout simulations of the filter. Figure 7.1 to 7.6 show the single amplitude transfer function of Cell 1, 2 and 3 for both cases of 10 MHz and 20 MHz bandwidth. It is clear that the designed circuit is able to reproduce the ideal filter. Also, it is possible to notice some cases in which a zero is present in the transfer function. This is caused by the Gate to Source capacitance of the transistor M1 and there are techniques that allows to compensate for it [18].

Figure 7.7 to 7.10 present the transfer functions of the full sixth order Chebyshev Type I LPF. Albeit with some imperfections, the circuit is capable to correctly implement the Chebyshev LPF for both 10 MHz and 20 MHz bandwidth.

Figure 7.11 and Figure 7.12 show also the phase of the transfer functions. Except for an initial phase shift of  $180^\circ$ , the results match the ideal phase behaviour. As already said in Chapter 3, it is important to have a linear trend of the phase in a linear plot so that each sub-carrier is exposed to the same relative phase shift.

Figure 7.13 and Figure 7.14 are retrieved through noise analysis. The behaviour of the input referred noise is displayed. Integrating over the bandwidths it is possible to compute the noise floor and Input-Referred Noise (IRN) of the filter.

In case of 10 MHz bandwidth, the noise floor is  $420 \mu\text{V}_{\text{RMS}}$  or  $-55 \text{ dBm}$  and  $\text{IRN} = 134 \text{ nV}_{\text{RMS}}/\sqrt{\text{Hz}}$ .

In case of 20 MHz bandwidth, the noise floor is  $350 \mu\text{V}_{\text{RMS}}$  or  $-56 \text{ dBm}$  and  $\text{IRN} = 78 \text{ nV}_{\text{RMS}}/\sqrt{\text{Hz}}$ .

Through transient analysis it is possible to retrieve also the value of the 1 dB compression point  $P_{1dB}$  and consequently of the IIP3 [5]. The filter achieves a  $P_{1dB} = -10 \text{ dBm}$  and an  $\text{IIP3} = 5 \text{ dBm}$  With respect to other works on SF filters it seems that the values related to linearity are quite low. The cause of this difference comes

from Cell 1. As already explained in the Design challenges section of Chapter 5, resistor  $R_1$  allows current flowing from one branch of the fully-differential circuit to the other one.  $R_1$  has been increased as much as possible in order to increase the linearity and as a consequence also the dynamic range. However this is currently the best result achieved from this configuration.

As a verification, the linearity analysis of the stand-alone Cell 2 and 3 provided a  $P_{1dB} = 18 - 20$  dBm.

### 7.3 Comparison with Wi-Fi requirements

The characteristics of the LPF can be compared with the requirements by following the list presented in Chapter 3:

- **Bandwidth:** 802.11ax will require base-band bandwidths of 10, 20, 40, 80 MHz. This work supports only bandwidths of 10 and 20 MHz because it is unlikely that the largest bandwidths can be consistently used in IoT applications.
- **Type and Order:** As repeatedly written throughout this text, the constraints on the filter selectivity impose to have at least a sixth order Chebyshev Type I LPF with a 3 dB ripple in the pass-band. This is the chosen filter designed in this work.
- **Linearity:** The minimum 1 db compression point required in the 802.11ax standard is  $P_{1dB} = -18.6$  dBm. This work obtains a  $P_{1dB} = -10$  dBm.
- **Noise:** The computed noise floor of the circuit is -52 dBm, remembering that a gain of 30 dB from the LNA and Mixer components is considered. The obtained noise floor is -55 dBm for a cut-off frequency of 10 MHz and -56 dBm for the 20 MHz one.
- **Dynamic range:** 802.11ax requires a dynamic range of 52 dB. The obtained filter dynamic range is 45-46 dB. This value results from the ratio of the 1 dB compression point ( $P_{1dB} = -10$  dBm) and the noise floor (-55 dBm at 10 MHz, -56 dBm at 20 MHz).

All the requirements except for the dynamic range are respected. The consequence of the dynamic range is that, depending also on the gain of the LNA, the filter is not able to support all the modulation that the standard does. A solution for this problem can be to increase the power consumption of the circuit in order to lower the noise floor or to change Cell 1 with a more linear cell based on Super SF like Cell 2 or Cell 3. However, it is still possible to use this filter for 802.11ax standard using LNA configurations that are capable of changing their gain according to the operating conditions [19].

As a last note, the area of the circuit is  $0.015 \text{ mm}^2$  and it consumes  $48 \text{ }\mu\text{W}$  for 10 MHz operation and  $121.5 \text{ }\mu\text{W}$  for 20 MHz operation.

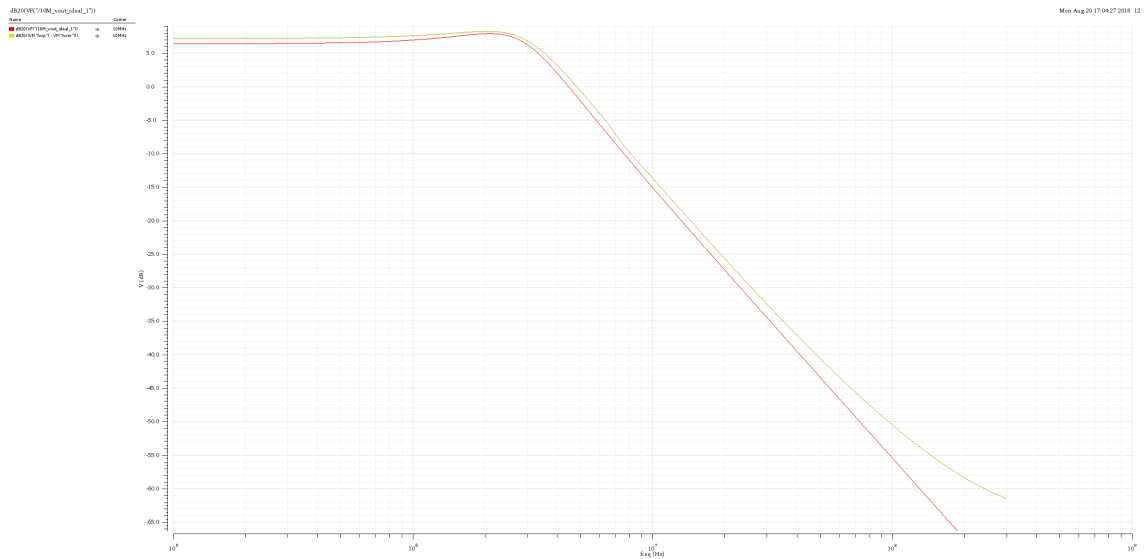


Figure 7.1: **Ideal** vs **post layout** amplitude transfer function of the first biquadratic cell, when cut-off frequency of the filter is set to 10 MHz.

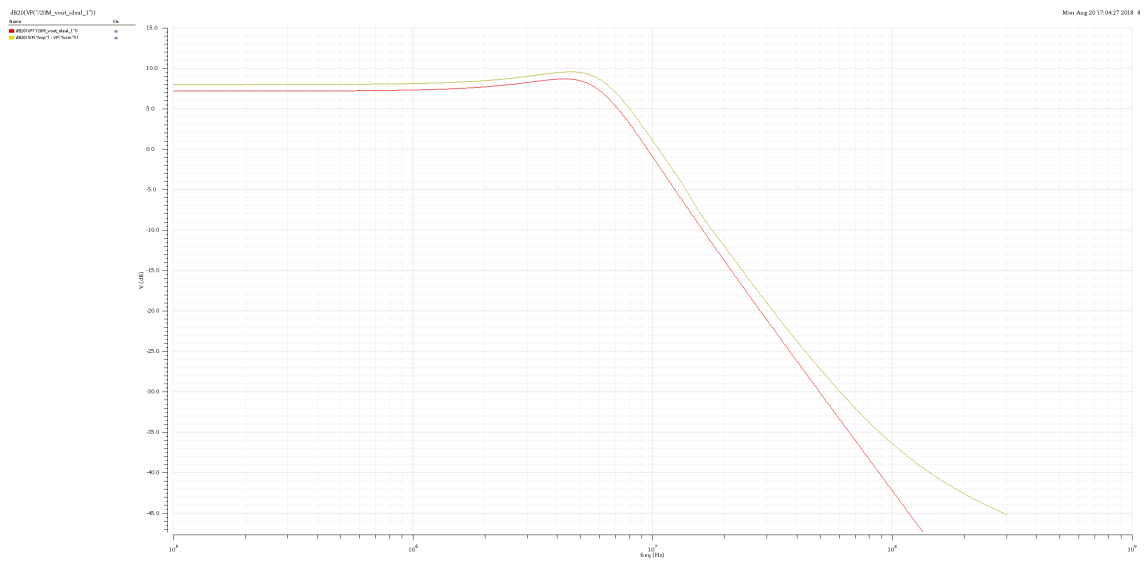


Figure 7.2: **Ideal** vs **post layout** amplitude transfer function of the first biquadratic cell, when cut-off frequency of the filter is set to 20 MHz.

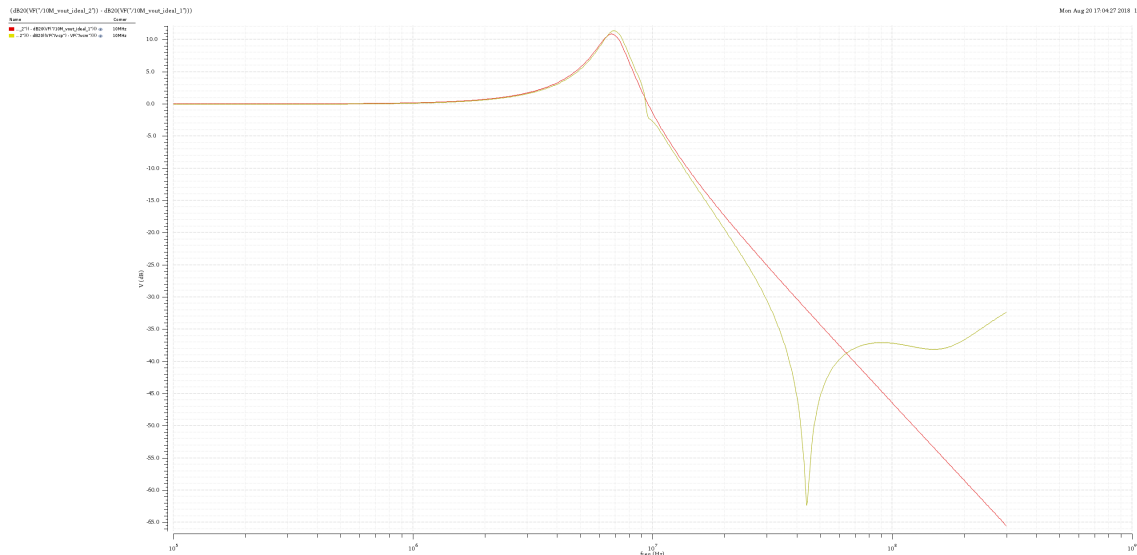


Figure 7.3: **Ideal** vs **post layout** amplitude transfer function of the second biquadratic cell, when cut-off frequency of the filter is set to 10 MHz.

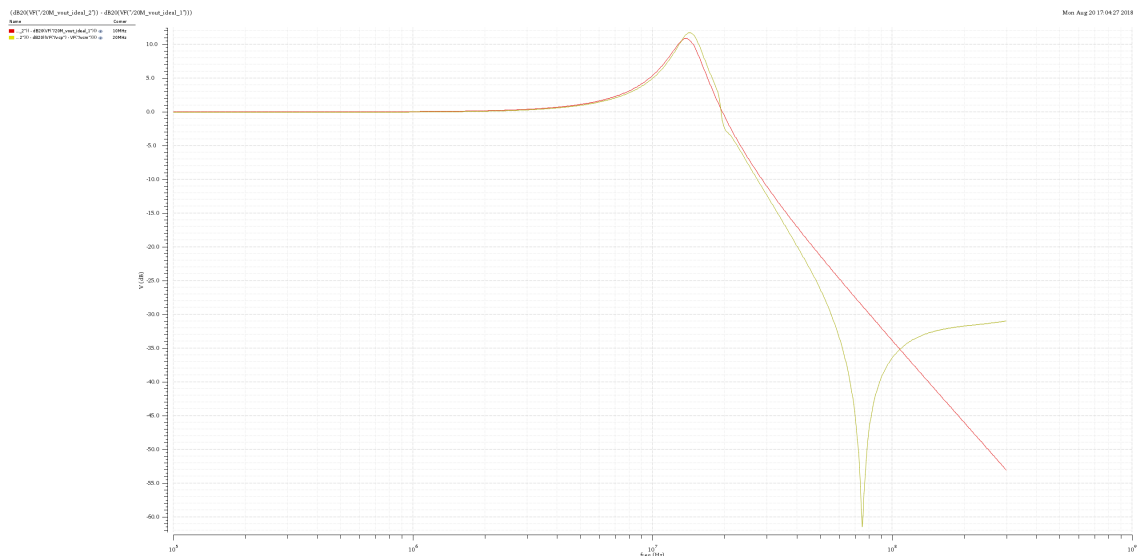


Figure 7.4: **Ideal** vs **post layout** amplitude transfer function of the second biquadratic cell, when cut-off frequency of the filter is set to 20 MHz.

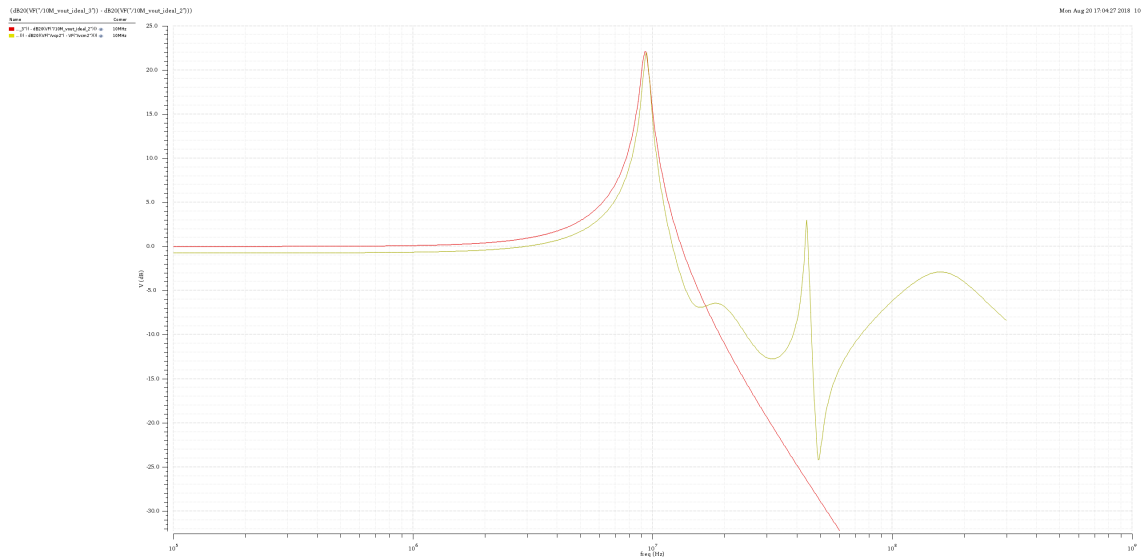


Figure 7.5: **Ideal** vs **post layout** amplitude transfer function of the third biquadratic cell, when cut-off frequency of the filter is set to 10 MHz.

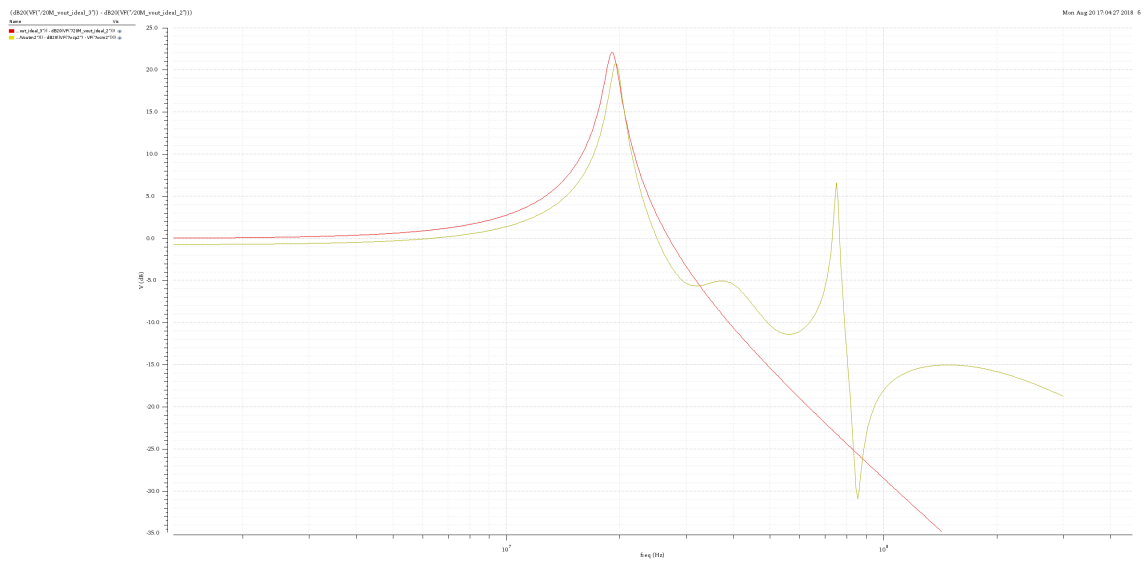


Figure 7.6: **Ideal** vs **post layout** amplitude transfer function of the third biquadratic cell, when cut-off frequency of the filter is set to 20 MHz.

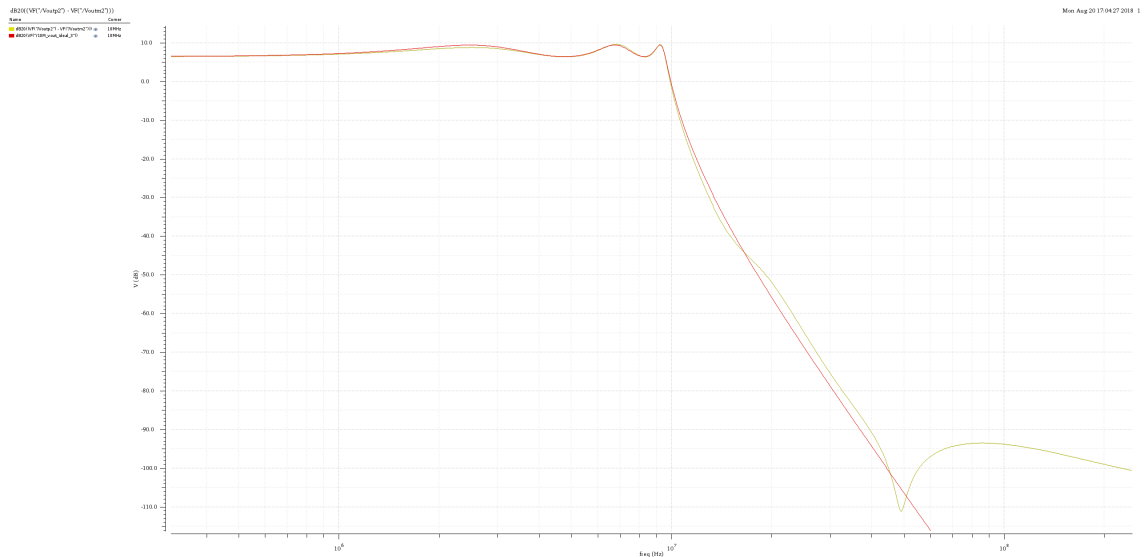


Figure 7.7: **Ideal** vs **post layout** amplitude transfer function of the entire system, when cut-off frequency of the filter is set to 10 MHz.

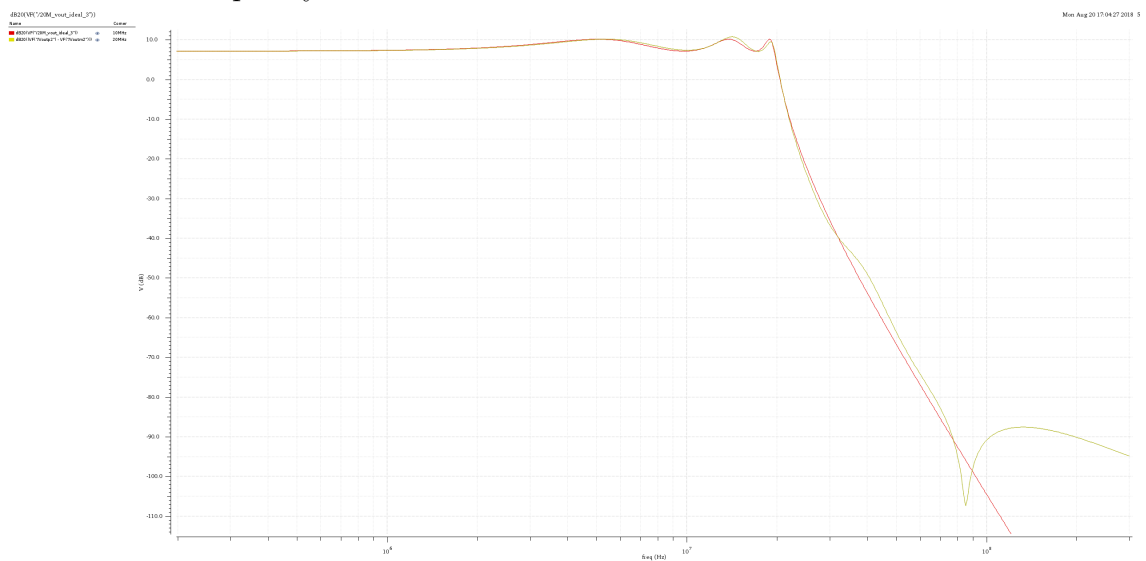


Figure 7.8: **Ideal** vs **post layout** amplitude transfer function of the the entire system, when cut-off frequency of the filter is set to 20 MHz.

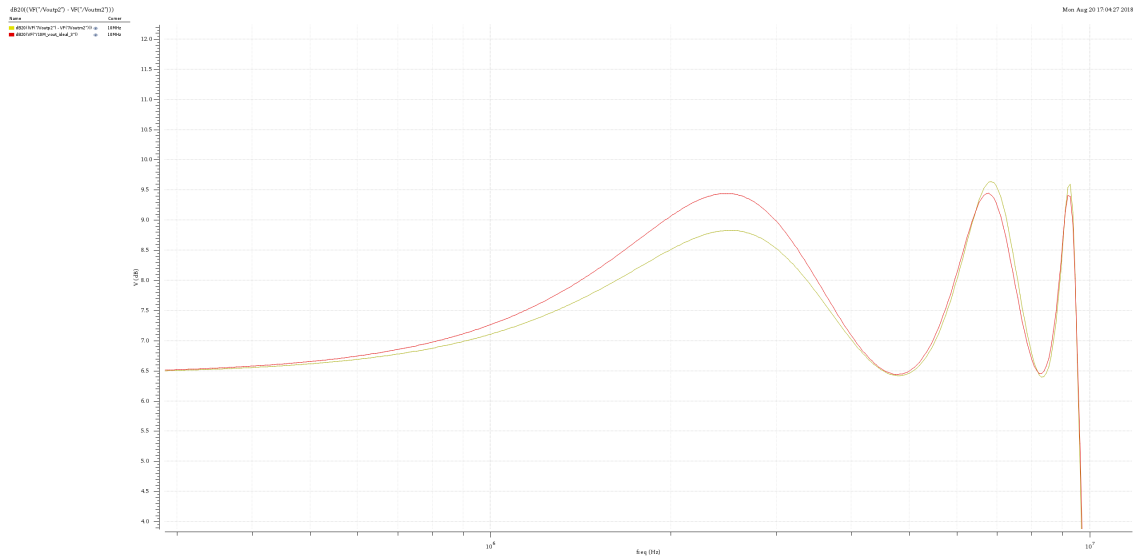


Figure 7.9: Detail of the pass band ripple of Figure 7.7.

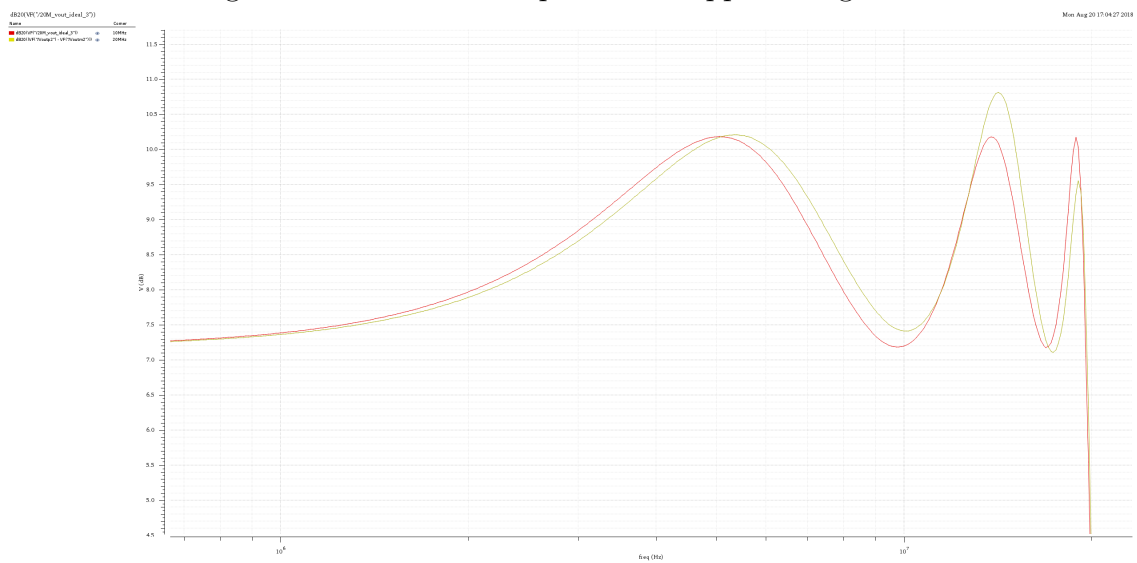


Figure 7.10: Detail of the pass band ripple of Figure 7.8.

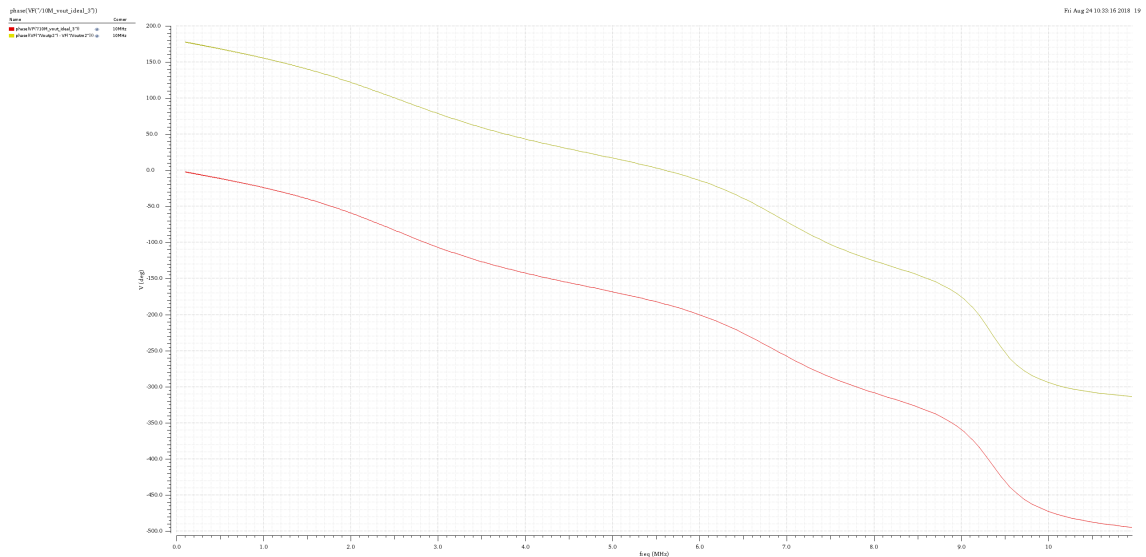


Figure 7.11: **Ideal** vs **post layout** phase transfer function of the entire system in linear scale, when cut-off frequency of the filter is set to 10 MHz.

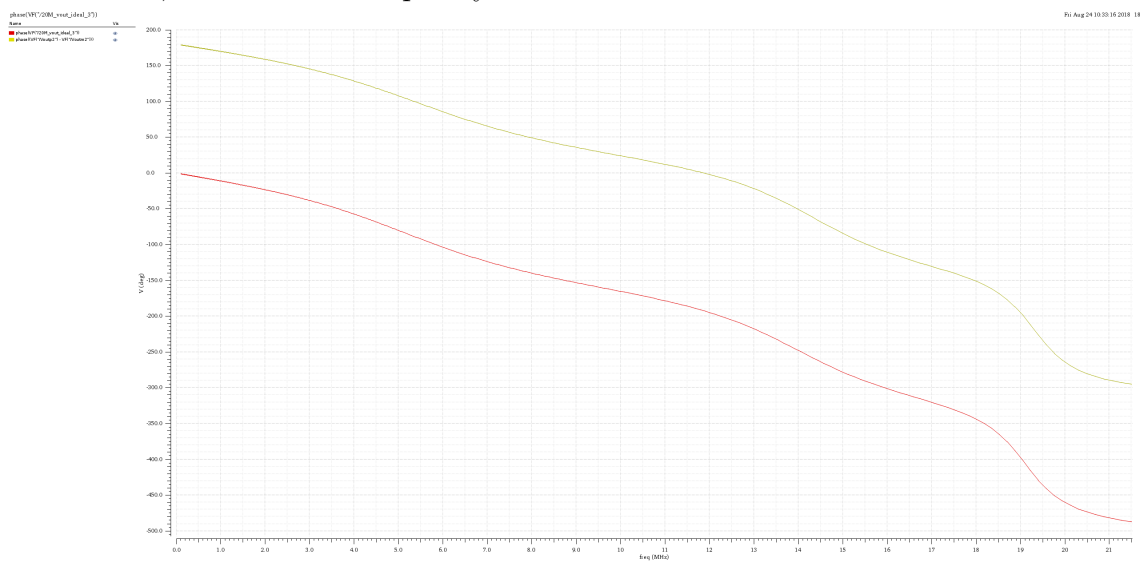


Figure 7.12: **Ideal** vs **post layout** amplitude transfer function of the the entire system in linear scale, when cut-off frequency of the filter is set to 20 MHz.

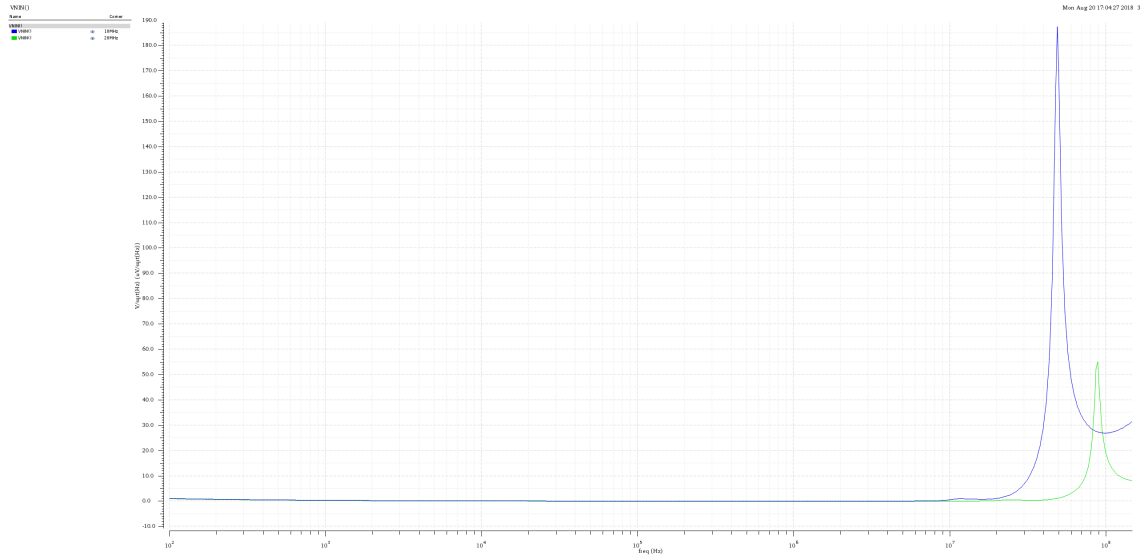


Figure 7.13: Input referred noise ( $\mu\text{V}/\sqrt{\text{Hz}}$ ) of the system for 10 MHz and 20 MHz.

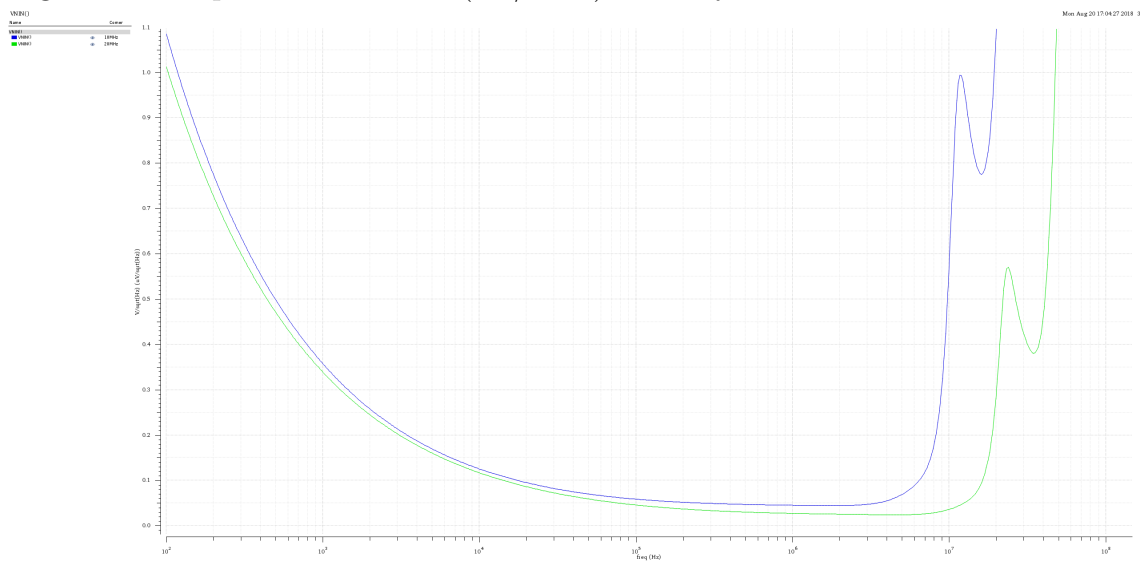


Figure 7.14: Detail of the input referred noise shown in Figure 7.13.

## 7.4 Comparison with state-of-the-art

Table 7.1 shows how the filter designed in this work compares with the current state-of-the-art of LPF. However, not all of these works target specifically wireless applications even though their characteristics are similar. The Figure-of-Merit (FoM) presented in Equation 7.1 is used in order to evaluate the quality of the filter [13] [20].

$$FoM = 10 \cdot \log \left( \frac{\left( \frac{IIP3}{V_{noise,in}} \right)^{4/3} \cdot f_c \cdot N}{P_W} \right) \quad (7.1)$$

In Equation 7.1 the following parameters appear:  $IIP3$  is the input level projection of the third order intercept point,  $V_{noise,in}$  corresponds to the noise floor in  $V_{RMS}$ ,  $P_W$  is the power consumption of the circuit,  $f_c$  is the cut-off frequency of the filter and  $N$  its order.

Parameter	[6]	[7]	[8]	[9]	[10]	[11]	[12]	[13]	[18]	This work
Technology (nm)	130	180	90	130	120	130	180	180	180	28
Supply voltage (V)	1.2	1.2	1	1	1	1.5	1.8	1.8	1.3	0.9
Architecture	OTA-C	$G_m$ -C	$G_m$ -C	active-RC	active-RC	active-RC	SF	SF	SF	SF
Order	2	3	6	5	5	5	4	4	5	6
Bandwidth (MHz)	200	0.5/20	8.1/13.5	20	5/10	19.7	10	33	20	10/20
Power (mW)	20.8	4.1/11	4.35	7.5	4.6	11.25	4.1	1.38	0.65	0.047/0.121
$P_{1dB}$ (dBm)	-	-	7.6	-	3.6	5	5	8	7.3	-10
IIP3 (dBm)	14	22.3/19	21.7/22.1	26	18.8/21.3	18.3	17.5	18	28.8	5
IRN ( $\text{nV}_{\text{RMS}}/\sqrt{\text{Hz}}$ )	35	425/12	75	52	143/85.4	30	7.6	7.83	15.3	134/78
Noise floor ( $\mu\text{V}_{\text{RMS}}$ )	494	301/54	213/276	232	320/270	133	24	45	68	425/350
Area ( $\text{mm}^2$ )	0.5	0.23	0.24	1.53	0.25	0.2	0.26	0.14	0.12	0.015
FoM	148	139/158	155/156	158	148/153	155	164	171	178	161

Table 7.1: Comparison of the characteristics of the simulated filter with respect to the measurements from the state-of-the-art



# Chapter 8

## Conclusion

The goal of this project has been to design a sixth-order Chebyshev Type I Low-Pass Filter for the next-generation of Wi-Fi (802.11ax) working at the frequencies of 10 and 20 MHz.

Three biquadratic cell based on new implementations of Source Follower filters have been used in order to design this filter. Cell 1 implements a fully differential second order filter based on Flipped Source Follower having 6 dB of DC Gain. Cell 2 and 3 implement two fully differential second order filters based on Super Source Follower capable of high quality factors.

The filter design has been carried out in a 28 nm technology provided by TSMC.

### 8.1 Performance

The designed filter presents the following characteristics:

- **Type and order:** sixth-order Chebyshev Type I Low-Pass Filter with 3 dB ripple in the pass-band.
- **Bandwidth:** reconfigurable between 10 MHz and 20 MHz.
- **DC Gain:** 6 dB provided by Cell 1.
- **Linearity:**  $P_{1dB} = -10$  dBm, IIP3 = 5 dBm
- **Noise:** Obtained noise floor is -55 dBm for 10 MHz bandwidth, -56 dBm in the case of 20 MHz bandwidth.
- **Dynamic range:** 45 dBm for 10 MHz bandwidth, 46 dBm in the case of 20 MHz bandwidth.
- **Power consumption:** 48  $\mu$ W for 10 MHz bandwidth, 121.5  $\mu$ W in the case of 20 MHz bandwidth.
- **Area:** 0.015 mm<sup>2</sup>

## 8.2 Future improvements

The part of the filter which needs bigger improvement is Cell 1 without any doubt. This cell is very small compared to Cell 2 and 3, however it is difficult to deal with in the design stage. An option would be to simplify the design of this cell using the Super SF topology instead of the Flipped SF. In addition, the gain provided by Cell 1 is helpful to compensate the small losses on Cell 2 and 3 and to reduce the noise generated by these cells. However, the resistors  $R_1, R_2$  provide the gain but limit the design space and especially the linearity of the filter. The equivalent implementation of Cell 1 in a Super SF topology could be used in order to increase the design space. Furthermore, a virtual ground could be introduced at the centre of resistor  $R_1$  in order to limit the current flowing from one side to the other of this component, possibly increasing the linearity of the filter.

Cell 2 could also be designed without the cascode transistor in order to reduce its area.

## 8.3 Next steps

In order for this circuit to be ready for tape-out few components need to be added. In particular, it is very important to add an output buffer in order to drive the load of the pads. This output buffer could be easily implemented by a source follower circuit.

In order to compensate for process variations it can be helpful to add few spare capacitances, a simple digital circuit to regulate the actual value of the capacitor would also be required.

This work is expected to be sent for tape-out in October.



# Appendix A

## Matlab design and sizing

This appendix shows an example of Matlab script used to design one of the three cells, in particular Cell 2 or 3. This code provides all the possible real solutions to the system according to the ranges of parameters chosen.

```
1  clc
2  close all
3  clear all
4
5  U_t = 1.38e-23*300/1.602e-19;
6  I_spec_square_n = 718.25e-9;
7  I_spec_square_p = 208e-9;
8  V_th_n = 0.32;
9  V_th_p = 0.38;
10 R_noise = 200*8;
11 gamma_nD = 0.5;
12
13 i=0;
14 j = 0;
15 BandWidth = 10e6
16 Vdd = 0.9;
17 cut_off_freq = 0.9772165;
18 W = cut_off_freq*2*pi*BandWidth;
19 n = 1.15;
20 L = 500e-9;
21 L_sat = 15e-9;
22 lambda_c = L_sat/L;
23 Lp = L;
24 np = 1.2;
25 lambda_c_p = L_sat/(Lp);
26
27 for V_gs2 = linspace(0.3,0.6,15)
28   V_gs3_p = Vdd-V_gs2;
29   for G_m1 = linspace(200e-6,400e-6,3)
30     G_ds1 = 0;
31     G_m3p = 1;
32     for G_m2 = linspace(50e-6,150e-6,3)
```

```

33 Q = 12.8
34 lastwarn('')
35 syms C_1_vect C_2_vect
36 sol = solve( 1/(W) == sqrt( C_2_vect*C_1_vect/(G_m2*
    G_m1*n)), 1/(W*Q) == (G_ds1*C_1_vect+C_2_vect*G_m2)
    /(G_m2*G_m1*n) , C_2_vect , C_1_vect);
37 [warnMsg, warnId] = lastwarn;
38 if isempty(warnMsg)
39     C_1 = 0;
40     C_1_vect = double(sol.C_1_vect);
41     if numel(C_1_vect)>1
42         for k=1:size(C_1_vect)
43             if (imag(C_1_vect(k)) == 0 && C_1_vect(k) > 0)
44                 C_1 = C_1_vect(k);
45             end
46         end
47     else
48         C_1 = C_1_vect;
49     end
50     C_2 = 0;
51     C_2_vect = double(sol.C_2_vect);
52     if numel(C_2_vect)>1
53         for k=1:size(C_2_vect)
54             if (imag(C_2_vect(k)) == 0 && C_2_vect(k) > 0)
55                 C_2 = C_2_vect(k);
56             end
57         end
58     else
59         C_2 = C_2_vect;
60     end
61     if (G_m1 ~= 0 && C_1 ~= 0 && C_2 ~= 0 && G_m2 ~= 0 &&
        G_m3p ~= 0)
62         G_m3_buf = G_m3p;
63         G_m2_buf = G_m2;
64         C_2_buf = C_2;
65         for kk=1:size(G_m3_buf)
66             G_m3p = G_m3_buf(kk);
67             G_m2 = G_m2_buf(kk);
68             C_2 = C_2_buf(kk);
69             syms IC2
70             IC2 = double(vpasolve((V_gs2 - V_th_n)/(n*U_t) ==
                -(1+log(2))+log(sqrt((1+lambda_c*IC2)^2 + 4*IC2)
                ) - 1) + sqrt((1+lambda_c*IC2)^2 + 4*IC2), IC2))
                ;
71             I_bias = 0;
72             I_bias = ( G_m2*IC2*n*U_t*(2+lambda_c+IC2*lambda_c
                ^2) ) / ( (-1 + sqrt( 4*IC2 + (1+IC2*lambda_c)
                ^2 ) ) ) ; % % % %

```

```

73
74 [warnMsg, warnId] = lastwarn;
75 if isempty(warnMsg)
76     W2 = (I_bias*L)/(I_spec_square_n*IC2);
77     syms IC1_vect
78     IC1_v = double(solve((n*G_m1*U_t)/(I_bias) == (
79         sqrt((1+lambda_c*IC1_vect)^2 + 4*IC1_vect)-1)
80         /(IC1_vect*(2+lambda_c*(1+lambda_c*IC1_vect))
81         ),IC1_vect));
82     [warnMsg, warnId] = lastwarn;
83     IC1 = 0;
84     if isempty(warnMsg)
85         if numel(IC1_v)>1
86             for k=1:size(IC1_v)
87                 if (imag(IC1_v(k)) == 0 && IC1_v(k) > 0)
88                     IC1 = IC1_v(k);
89                 end
90             end
91         else
92             IC1 = IC1_v;
93         end
94     if (IC1 ~= 0)
95         W1 = (I_bias*L)/(I_spec_square_n*IC1);
96         syms V_gs1
97         V_gs1 = double(vpasolve((V_gs1 - V_th_n)/(n*
98             U_t) == -(1+log(2))+log(sqrt((1+lambda_c*
99             IC1)^2 + 4*IC1) - 1) + sqrt((1+lambda_c*
100             IC1)^2 + 4*IC1),V_gs1));
101
102     syms IC3p
103     IC3p = real(double(vpasolve((V_gs3_p -
104         V_th_p)/(np*U_t) == -(1+log(2))+log(sqrt
105         ((1+lambda_c_p*IC3p)^2 + 4*IC3p) - 1) +
106         sqrt((1+lambda_c_p*IC3p)^2 + 4*IC3p),IC3p
107         )));
108     I_bias_p = ( IC3p*np*G_m3p*U_t*(2+lambda_c_p
109         +IC3p*lambda_c_p^2) ) / ( -1 + sqrt( 4*
110         IC3p + (1+IC3p*lambda_c_p)^2 ) );
111     W3p = (I_bias_p*(Lp))/(I_spec_square_p*IC3p)
112         ;
113
114     V_gs4 = 0.9 - V_gs1;
115     if (V_gs4 > 0)
116         syms IC4
117         IC4 = real(double(vpasolve((V_gs4 - V_th_n
118             )/(n*U_t) == -(1+log(2))+log(sqrt((1+
119             lambda_c*IC4)^2 + 4*IC4) - 1) + sqrt
120             ((1+lambda_c*IC4)^2 + 4*IC4),IC4)));

```

```

105     W4 = (I_bias_p*L)/(I_spec_square_n*IC4);
106
107     if isempty(warnMsg) && ~isa(W1, 'sym') && ~
108         isa(IC1, 'sym')
109         if (IC1 > 0 && W1 > 0 && IC2 > 0 && W2
110             > 0 && IC3p > 0 && W3p > 0)
111             i=i+1;
112             BandWidth_Vect(i) = BandWidth;
113             I_b(i) = I_bias;
114             I_bias_p_Vect(i) = I_bias_p;
115             Gm1_Vect(i) = G_m1;
116             Gm2_Vect(i) = G_m2;
117             Gm3p_Vect(i) = G_m3p;
118             Diff_G_m23_Vect(i) = G_m3p - G_m2;
119             C1_Vect(i) = C_1;
120             C2_Vect(i) = C_2;
121             IC1_Vect(i) = IC1;
122             IC2_Vect(i) = IC2;
123             IC3p_Vect(i) = IC3p;
124             W1_Vect(i) = W1;
125             W2_Vect(i) = W2;
126             W3p_Vect(i) = W3p;
127             W4_Vect(i) = W4;
128             V_gs1_Vect(i) = V_gs1;
129             V_gs2_Vect(i) = V_gs2;
130             V_gs3_p_Vect(i) = V_gs3_p;
131             Q_Vect(i) = Q;
132         end
133     end
134 end
135 end
136 end
137 end
138 end
139 end
140     j = j+1;
141 end
142 end
143 end
144
145 BandWidth_Vect = transpose(BandWidth_Vect);
146 I_b = transpose(I_b);
147 I_bias_p_Vect = transpose(I_bias_p_Vect);
148 Gm1_Vect = transpose(Gm1_Vect);
149 Gm2_Vect = transpose(Gm2_Vect);

```

```

151 Gm3p_Vect = transpose(Gm3p_Vect);
152 Diff_G_m23_Vect = transpose(Diff_G_m23_Vect);
153 C1_Vect = transpose(C1_Vect);
154 C2_Vect = transpose(C2_Vect);
155 IC1_Vect = transpose(IC1_Vect);
156 IC2_Vect = transpose(IC2_Vect);
157 IC3p_Vect = transpose(IC3p_Vect);
158 W1_Vect = transpose(W1_Vect);
159 W2_Vect = transpose(W2_Vect);
160 W3p_Vect = transpose(W3p_Vect);
161 W4_Vect = transpose(W4_Vect);
162 V_gs1_Vect = transpose(V_gs1_Vect);
163 V_gs2_Vect = transpose(V_gs2_Vect);
164 V_gs3_p_Vect = transpose(V_gs3_p_Vect);
165 Q_Vect = transpose(Q_Vect);
166
167 csv_row_matrix =[BandWidth_Vect , I_b , I_bias_p_Vect , Gm1_Vect ,
    Gm2_Vect , Gm3p_Vect , Diff_G_m23_Vect , C1_Vect , C2_Vect ,
    IC1_Vect , IC2_Vect , IC3p_Vect , W1_Vect , W2_Vect , W3p_Vect ,
    W4_Vect , V_gs1_Vect , V_gs2_Vect , V_gs3_p_Vect , Q_Vect ];
168
169 dlmwrite( 'cell_parameters.dat' , csv_row_matrix );

```



# Bibliography

- [1] “IEEE Std 802.11-2016 (Revision of IEEE Std 802.11-2012)”. In: *IEEE Xplore* (2016).
- [2] “IEEE Std 802.11ax (Draft 2.1) - Specification Framework for TGax”. In: *IEEE Xplore* (2017).
- [3] National Instruments. *Introduction to WLAN Testing*. URL: [www.ni.com/rf-academy](http://www.ni.com/rf-academy).
- [4] Behzad Razavi. *RF microelectronics*. 2nd ed. Upper Saddle River, NJ: Prentice Hall, 2012.
- [5] C. C. Enz. *Lecture notes in HF and VHF Circuits and Techniques I*. EPFL, 2017.
- [6] M. Mobarak et al. “Attenuation-predistortion linearization of CMOS OTAs with digital correction of process variations in OTA-C filter applications”. In: *IEEE J. Solid-State Circuits* 45.2 (2010), pp. 351–367.
- [7] T. Lo, C. Hung, and M. Ismail. “A wide tuning range gm-C filter for multi-mode CMOS direct-conversion wireless receivers”. In: *IEEE J. Solid-State Circuits* 44.9 (2009), 2515–2524.
- [8] M. Oskooei et al. “A CMOS 4.35-mW 22-dBm IIP3 continuously tunable channel select filter for WLAN/WiMAX receivers”. In: *IEEE J. Solid-State Circuits* 46.6 (2011), 1382–1391.
- [9] H. Amir-Aslanzadeh, E. Pankratz, and E. Sanchez-Sinencio. “A 1-V 31 dBm IIP3, reconfigurable, continuously tunable, power-adjustable active-RC LPF”. In: *IEEE J. Solid-State Circuits* 44.2 (2009), pp. 495–508.
- [10] A. Vasilopoulos et al. “A low-power wideband reconfigurable integrated active-RC filter with 73 dB SFDR”. In: *IEEE J. Solid-State Circuits* 41.9 (2006), pp. 1997–2008.
- [11] S. Kousai et al. “A 19.7MHz, fifth-order active-RC chebyshev LPF for draft IEEE802.11n with automatic quality factor tuning scheme”. In: *IEEE J. Solid-State Circuits* 42.11 (2007), 2326–2337.
- [12] S. D’Amico, M. Conta, and A. Baschirotto. “A 4.1-mW 10-MHz Fourth-Order Source-Follower-Based Continuous-Time Filter With 79-dB DR”. In: *IEEE Journal of Solid-State Circuits* 41.12 (2006), pp. 2713–2719.
- [13] M. De Matteis et al. “A 33 MHz 70 dB-SNR Super-Source-Follower-Based Low-Pass Analog Filter”. In: *IEEE Journal of Solid-State Circuits* 50.7 (2015), pp. 1516–1524.

- [14] M. De Matteis and A. Baschirotto. “A Biquadratic Cell Based on the Flipped-Source-Follower Circuit”. In: *IEEE Transactions on Circuits and Systems II: Express Briefs* 64.8 (2017), pp. 867–871.
- [15] Larry D. Paarmann. *Design and Analysis of Analog Filters - A Signal Processing Perspective*. 1st ed. Vol. 617. The Kluwer International Series in Engineering and Computer Science. Kluwer Academic Publishers, 2001.
- [16] Eric A. Vittoz Christian C. Enz. *Charge-Based MOS Transistor Modeling: The EKV Model for Low-Power and RF IC Design*. Wiley, 2006.
- [17] C. C. Enz. *Lecture notes in Advanced Analog and RF IC Design I*. EPFL. 2017.
- [18] Y. Xu, J. Muhlestein, and U. Moon. “A 0.65mW 20MHz 5th-order low-pass filter with +28.8dBm IIP3 using source follower coupling”. In: *IEEE Custom Integrated Circuits Conference* (2017).
- [19] M. Ganesh Lakshmana Kumar et al. “Design of current reuse based Differential Merged LNA-Mixer (DMLNAM) and two-stage Dual Band LNA with two gain modes in 65nm technology”. In: *IEEE Asia Pacific Conference on Post-graduate Research in Microelectronics and Electronics (PrimeAsia)* (2015), 98–103.
- [20] W. Sansen. “Analog design challenges in nanometer CMOS technologies”. In: *IEEE Asian Solid-State Circuits Conference* (2007), pp. 5–9.

